INVESTIGATION OF SUBMARINE LANDSLIDE DEPOSITS ALONG THE NORTHERN MARGIN OF PUERTO RICO

Meghan E. Hearne

A Thesis Submitted to the
University of North Carolina at Wilmington in Partial Fulfillment
Of the Requirements for the Degree of
Master of Science

Department of Earth Sciences

University of North Carolina at Wilmington

2004

Approved by

Advisory Committee

_____ _____

_____
Chair

Accepted by

_____
Dean, Graduate School

This document has been prepared according to the guidelines for submission to the Journal of Marine Geology.

TABLE OF CONTENTS

ABSTRACT

The seismogenic northeastern North America-Caribbean oblique-slip plate boundary includes the 8.5-km deep Puerto Rico trench, 120 km north of the densely populated islands of Puerto Rico and the Virgin Islands. The northern insular margin of Puerto Rico, adjacent to the Puerto Rico trench, is characterized by frequent seismicity, rapid Neogene trenchward tilting, and oversteepened slopes. Multibeam bathymetry, sidescan sonar, and single-channel seismic reflection data reveal extensive submarine landslide deposits on the margin that can be traced upslope to two large (up to 55-km wide and 6.1-km deep) amphitheater-shaped headscarps along the edge of the Puerto Rico –Virgin Islands (PRVI) carbonate platform. The crown of the larger, westernmost scarp incises the platform at 2600 meters below sea level, ~ 40 km off the north coast of Puerto Rico. The associated submarine landslide deposits extend up to 80 km trenchward, covering a total seafloor area of 4313 km^2. Seismic reflection data show a maximum debris deposit thickness of 2850 m. The debris deposit consists of multiple layers each approximately 200 m thick. This suggests that the slope failure may have occurred as multiple failure events, rather than a single catastrophic event. Allowing for compaction of the debris deposit sediments, the volume of 1378 km^3 for the amphitheater is comparable to the calculated compacted landslide debris volume of 1426 km^3. These results suggest that the collection of submarine landslide units is associated with the formation of the giant amphitheater over time. This also suggests that the debris is not being removed by translation or subduction, unlike other convergent margins. Although the exact triggering mechanism(s) for the submarine landslides is not known, tectonic erosion related to the westward migration of the overthickened (20+ km) southeastern Bahamas Province beneath the PRVI margin is a likely candidate. The present-day collision zone is interpreted to be offshore northwestern Puerto Rico, an area characterized by

mid-slope uplift, anomalously high seismicity and crescentic cracks in the PRVI carbonate platform that are similar in size and shape to amphitheaters observed further to the east. Evidence of multiple, Pliestocene and younger submarine landslide deposits adjacent to the uplifted Mona Block and within the Mona Rift suggest that the devastating 1918 tsunami could have been generated by a seismically triggered submarine landslide. Moreover, the proximity of crescentic-shaped seafloor cracks to the tectonically active Mona Rift make them likely candidates for sites of future breakaway scarps and catastrophic submarine landslides. A modern day inundation would have detrimental effects on Puerto Rico whose population has dramatically increased over the past century to about 3.89 million.

ACKNOWLEDGMENTS

Thanks go to Dr. Jack Hall whose enthusiasm in Earth and Environmental Science first sparked my interest in geology. I would like to thank all of the faculty members in the Earth Science department that contributed to my education, whether you were my teacher or a resource.

I am especially thankful to have been welcomed as a graduate student in the Coastal and Marine Geophysics Laboratory by my advisor Dr. Nancy R. Grindlay. Thank you Dr. Grindlay, for your encouragement and support, the incomprehensible amount of guidance you have provided me with throughout all of my research, and primarily, your patience (with me).

Thank you, Roger Shew, for taking the time to look over the seismic and sidescan data with me. I admire your expertise in geology and geophysics. I have learned so much from you.

Many thanks to Dr. Michael Freeze who miraculously taught me calculus at eight a.m. four days a week during the summer. Thank you for your interest in my research and the time you took to teach me how relevant mathematics was to everyday situations.

The Graduate School and the National Science Foundation are thanked for providing me with the financial support for my research.

Final thanks go to my thesis committee, Dr. Abrams, Dr. Smith, and Dr. Nancy R. Grindlay, for all the support and guidance you have provided me with throughout my time as undergraduate and graduate student, here at UNC Wilmington.

LIST OF TABLES

LIST OF FIGURES

INTRODUCTION

Submarine landslides can involve huge amounts of sediment removal, are often greater than their terrestrial counterparts, and have the potential to transport seafloor material great distances (Heezen and Ewing, 1952; Embley, 1982). The Agulhas submarine landslide off South Africa, the largest slope failure documented, involved a volume as large as 20,000 km^3 and a run out distance of greater than 140 km (Dingle, 1977). Such values suggest that submarine landslide events are a principal means of transferring terrigenous and shallow-water sediment into the deep ocean basins and in the sculpting of both continental and insular margins.

An important aspect of detailing submarine failures is to identify the potential for large volume, mass wasting events to be tsunamigenic. Depending on the size and speed of a submarine landslide, its distance from shore, the shape of the nearshore bathymetry and coastline, and other factors, submarine landslide events have the potential to generate a tsunami (Ward, 2001; Jiang and LeBlonde, 1992). With increasing global populations and the concentration of much of that population along coastal regions, these tsunamis can have significant deadly impact. For example, a 15-m high tsunami triggered by an earthquake and submarine landslide off the north coast of Papua New Guinea in 1998 killed more than 2,000 of the island's coastal inhabitants (Synolakis et al, 2002; Tappin, 2003). The northern insular margin of Puerto Rico and the Virgin Islands, where large (up to 55-km across) amphitheater-shaped scarps and submarine landslide deposits have been identified, may pose a similar hazard to the inhabitants of Puerto Rico, most of who live along the island's 501 km of coastline. A large earthquake (Mw = 7.3) that occurred on the 11 October 1918, ~ 15 km off the northwestern coast of the island of Puerto Rico was accompanied by a tsunami with a maximum run up along

the northwestern coast of the island (Figure 1). The greatest inundation was in the cities of Mayaguez and Aguadilla where observed run up exceeded 6 m (Reid and Taber, 1918; Mercado and McCann, 1998). The wave was responsible for over 100 deaths and nearly 50 million dollars of damage (2004 currency). The historical record of Puerto Rico confirms that the 1918 event was not the first tsunamigenic episode to impact the island. An earthquake of Mw = 7.5 accompanied by a tsunami struck the Virgin Islands and Puerto Rico in 1867. The most severely impacted islands were St. Thomas and St. Croix of the U.S. Virgin Islands where observed run up reached 7 m and casualties where in the hundreds (Mercado and McCann, 1998). A modern day event of comparable magnitude would have damaging effects on Puerto Rico whose combined population has dramatically increased over the past century to about 3.89 million (U.S. Census Bureau, 2002).

In this paper a high-resolution bathymetry, sidescan sonar, and single-channel seismic reflection data set is used to map surface and subsurface features of a giant amphitheater-shaped scarp on the northern insular margin of Puerto Rico. The volume of material and run out extent for a submarine landslide associated with the amphitheater are calculated. These data are also used to identify areas on the margin that are potential sites of future submarine landslides that are capable of generating a tsunami. Lastly, possible triggering mechanisms for submarine landslides along the northern Puerto Rico-Virgin Islands margin are discussed.

BACKGROUND

Submarine Landslide Identification

The identification of submarine mass movement types has been based on characteristic expressions documented by multibeam bathymetry, sidescan sonar, and high-resolution sub-bottom profiling (USGS Bulletin, 2002; Locat and Lee, 2002). Submarine landslides are identified by two characteristic features: a distinct headwall region (the rupture surface - the scarp itself) and the displaced mass (Hampton, 1972) (Figure 2a). Movement types represent a continuum from rock falls or avalanches to slow-moving creeps, to slumps and slides (rotational or translational), and to sediment gravity flows which range from matrix supported debris flows to turbidity currents (Figure 2b) (Morgenstern, 1967; Hampton, 1972; Varnes, 1978; Varnes and Cruden, 1996). At any point in time, the submarine landslide mass has the capability of evolving from one end of the morphology spectrum to the other, complicating the identification process. For example, a slide block may remain completely intact and proximal to the headwall, break up into smaller pieces, or disintegrate into a debris flow and widespread, turbidites in areas distal from the scarp (Hampton, 1972; Varnes, 1978; McAdoo, 2000).

Triggering Mechanisms

Depending upon location, a wide variety of processes have been identified as mechanisms that can contribute to sediment instability and potentially lead to submarine landslides (Hampton, 1972; von Huene, 1989; Moore, 1990; McAdoo, 2000; Lee et al., 2002; Locat and Lee, 2002). Whenever packages of sediment are subject to a force(s) that cause shear stress orientated downslope to exceed the shear strength of the material, the result is often a

downward and outward movement of the seafloor, or a submarine landslide (Embley, 1986; Hampton et al., 1996; McAdoo et al., 2000; Lee et al., 2002; Locat and Lee, 2002).

Although submarine landslides were once thought to occur most commonly along inclined areas of the seafloor, recent seafloor surveys show that these events can actually occur on passive margins where slopes are as low as 0.5 - 1° (Lee et al., 2002; Locat and Lee, 2002). Rapid deposition of unlithified, fine-grained sediment and rock and subsequent overloading can lead to elevated pore water pressure and sediment instability without extreme slopes. Small-scale seafloor erosion, such as carbonate dissolution beneath the calcium compensation depth and the presence of gas hydrate clathrates can result in grain-by-grain erosion of seafloor material (Lee et al., 2002). The small-scale erosion can lead to an increase in the slope gradient, thereby contributing to larger-scale landsliding along oversteepened slip planes (Lee et al., 2002). Tectonic erosion along active forearc regions and seismic strain imparted by earthquakes have been well documented as triggering mechanisms for episodes of large-scale, catastrophic submarine landslides (von Heune et al., 1989; von Heune and Ranero, 2001; Collot et al., 2001; Lastras et al., 2002).

STUDY AREA

Northeastern Caribbean-North America Plate Boundary Zone

The neoteconic setting of the northeastern Caribbean-North America plate boundary zone is complex. At least since the Pliocene, interactions between the North America and Caribbean lithospheric plates at the longitude of Puerto Rico involve oblique underthrusting to westward strike-slip movement of the ~ 100 m.y. old North Atlantic ocean crust along the Puerto Rico trench (Westbrook and McCann, 1986; Larue and Ryan, 1998). The Puerto Rico trench lies approximately 120 km north of the island of Puerto Rico and reaches depths up to 8450 m, forming the deepest seafloor feature in the Atlantic Ocean (Figure 3). The trench is also associated with the earth's largest negative (-350 mgal) free-air gravity anomaly (Bowin, 1972).

The most recent GPS-based geodesy and geological observations support oblique collision in the northeastern Caribbean, showing that the Caribbean plate moves 18-20 mm/yr east-northeastward (070º) relative to a fixed North America plate (Jansma et al., 2000; Mann et al., 2002; Calais et al., 2003) (Figure 1). Because of the highly oblique nature of convergence, strain is partitioned between the main thrust interface and at least two strike-slip fault zones within the overriding plate, Bunce and Bowin, that trend subparallel to the direction of relative plate motion (Figure 3) (Grindlay et al., 2004). The geodetic studies also indicate that E-W extension is occurring in the Mona Passage in response to the differential eastward movement of Puerto Rico relative to Hispaniola. Mann et al. (2002) suggest that the eastward motion of Hispaniola has been slowed by the collision of the southeastern Bahamas along its northern coast.

The northeastern Caribbean-North America plate boundary is characterized by a well-defined Wadati-Benioff zone that reflects the southerly dipping slab of North America lithosphere to depths of up to 180-200 km (McCann, 1985; Dillon et al., 1996; Dolan and Wald, 1998; McCann, 2002). Shallow earthquakes occurring along the interplate thrust zone have been considered likely to produce large earthquakes up to a magnitude 8 (McCann and Sykes 1984; Westbrook and McCann, 1986; McCann, 2002). Locations of concentrated and frequent earthquakes within the overriding Caribbean plate have been documented to occur near the Mona Rift off the northwest coast of Puerto Rico and in a NW-SE trending zone north of the Virgin Islands. This seismic activity has been attributed to deformation associated with the subduction of bathymetric highs on the North American plate (McCann and Sykes, 1984; McCann, 1985; Grindlay, et al., 2004).

Northern Puerto Rico - Virgin Islands Margin

The northern Puerto Rico – Virgin Islands (PRVI) margin is composed of Cretaceous to Lower Oligocene island arc basement volcanic and sedimentary rocks underlying a carbonate platform deposited during the early Oligocene to Pliocene. The carbonate platform was deposited over an area of approximately 18,000 km^2, extending from the eastern Dominican Republic on the island of Hispaniola toward the Virgin Islands area and southward where it outcrops on the island of Puerto Rico (Figure 3) (van Gestel et al., 1998).

The carbonate platform is composed of parallel beds of uniform carbonate units. These observations suggest that the platform was deposited during a tectonically quiet period (Moussa et al., 1987; Larue and Ryan, 1998; van Gestel et al., 1998; 1999). The laterally homogeneous carbonate layers dip northward at an average angle of 4-5° with maximum dip reaching up to 8°.

The carbonate platform extends northward, up to 60 km off the north coast of the island to water depths up to 6.5 km (Figure 4) (van Gestel et al., 1998; 1999). This discovery indicates substantial subsidence and oversteepening of the entire northern PRVI carbonate platform during the Neogene.

A preliminary marine geophysical survey using the GLORIA sidescan sonar system and widely spaced single-channel seismic reflection data first mapped a large, amphitheater-shaped indentation along the seaward edge of the PRVI carbonate platform, approximately 35-km north of Arecibo on the island of Puerto Rico (Schwab et al., 1991). The sidescan sonar imagery showed that the scarp was approximately 55-km wide and extended to the base of the slope. The abrupt termination of the carbonate platform reflectors at the amphitheater-shaped indentation suggests that extensive submarine landslides occurred along the otherwise relatively undisturbed carbonate platform northern margin. Schwab et al. (1991) estimated that the amphitheater represented the removal of up to 1500 km^3 of the PRVI carbonates.

MARINE GEOLOGICAL AND GEOPHYSICAL DATA

Regional mapping of the northern PRVI margin and the Puerto Rico Trench, was conducted aboard the *R/V Maurice Ewing* in June-July 1996 (EW96-05). Thirty-six, NNE-SSW ship tracks of single-channel seismic reflection data, sidescan sonar, multibeam bathymetry, gravity, and magnetics data were gathered giving a total along-track distance of 5600 km (Figure 3). Tracklines were closely spaced at 12 to 14 km.

Multibeam Bathymetry

The Atlas Hydrosweep multibeam bathymetry acquisition system transmits 59 acoustic beams at 15.5 kHz. The 90˚ swath coverage reaches up to twice the water depth and has a vertical and horizontal resolution of ~10 m and ~30 m, respectively. The Hydrosweep bathymetry data were gridded at a cell size of 250 m to produce the 2-D shaded relief images presented in this paper. The dense grid reveals the detailed morphology of the seafloor along the northern insular margin of Puerto Rico and the Puerto Rico trench (Figure 4a).

Sidescan Sonar Imagery

During the EW96-05 cruise the HAWA'II MR1 (HMR1) swath mapping system imaged ~ 50,000 km^2 of the seafloor. The HMR1 system is a wide swath (up to 20 km), shallow towed (100 mbsl), side-scanning instrument operating at a frequency of 11 kHz on its portside and 12 kHz on its starboard. An electrical problem in the tow fish caused significant degradation of the HMR1 bathymetry data for the majority of the cruise. The electrical problem affected the sidescan data as well. The contamination shows up on the starboard half of the swath as a band of track-parallel muted data, primarily in water depths greater than ~ 4500 m; however, the data

are still higher resolution (grid interval of 17m x 17m) than the previously gathered GLORIA sidescan sonar imagery of this area.

The intensity of the sidescan return signals depends on the angle of insonification and the texture of the seafloor surface. Hard rocks, fault scarps, and coarse-grained to disorganized debris of high backscatter intensity appear as dark grey-black colors. Fine-grained sediments, pelagic material, and relatively undisturbed slump packages of PRVI carbonate platform are characterized by low backscatter intensity and appear light grey in color (Figure 4b).

Single-channel Seismic Data

Thirty-six single-channel seismic reflection (SCS) profiles aligned NNE-SSW to the northern PRVI margin were gathered during the EW96-05 cruise. A six air gun array with 1385 ci capacity was towed along track with the HMR1 system. A four-channel streamer with an active section length of 137.5 m was used to record the seismic reflection data. EW96-05 cruise lines 3, 19, 20, 21, 23, and 26 used in this research were processed through full-migration (see van Gestel et al., 1998 for details). The profiles typically imaged up to 3.0 - 4.0 sec subsea floor. van Gestel et al. (1998; 1999) have documented good correlation between units imaged in the upper-slope of the northern PRVI margin and onshore core data of the PRVI carbonate platform.

The seismic data were used to identify the submarine landslide run out extent by the base-of-landslide horizon and to produce an isopach map of the entire submarine landslide debris field. In addition, the seismic profiles were used in combination with the sidescan sonar data to identify faults along the northern insular shelf and slope that might serve as planes of weakness for future landsliding of the platform carbonates and underlying volcaniclastics rocks.

Geologic Cores

Piston-core data from within the main Plain of the Puerto Rico trench and southern areas, including the Elevated Plain and northern insular slope of Puerto Rico, were taken during the *R/V Vema* (1956), the *R/V Conrad* (1964), and the *R/V Columbus Iselin* (1981) cruises (Table 1, Figure 4a). These cores have been used by researchers to determine sedimentation patterns offshore Puerto Rico and in the main trench axis (Conolly and Ewing, 1967; Doull, 1984; Pilkey and Cleary, 1985). The core data show that majority of the sediment in the Elevated and Main plains are turbidites and that up to 20% of the sediment is coarse sand and skeletal material from shallow-water sources (Connolly and Ewing, 1967; Doull, 1984; Pilkey and Cleary, 1985). Although core penetration was fairly shallow the deepest core penetrated the upper 9 m of seafloor. The cores show evidence of at least three Pleistocene and younger turbidite deposits that have been correlated for 10's of km across the lower Puerto Rico slope onto the trench axis (Conolly and Ewing, 1967; Doull, 1984; Pilkey and Cleary, 1985). One of the deposits, referred to as the Giant Elevated Plain Turbidite (EPT-3), represents a volume of up to 1.9 km^3 of shallow-water sand and shell fragments (Doull, 1984). Table 1 lists the core description of the EP-3 sand turbidite and overlying lutite turbidite sequences. The principle direction of turbidite transport was northward onto the Elevated Plain and then westward through an "abyssal gap" towards an inferred final deposition on the Main Plain. (Figure 4a) (Connolly and Ewing, 1967; Doull, 1984; Pilkey and Cleary, 1985).

MORPHOLOGY AND STRUCTURE OF SUBMARINE HEADSCARPS AND LANDSLIDE DEPOSITS

Amphitheater-Shaped Headscarps

Data collected during EW9605 cruise reveal two large amphitheater-shaped headscarps carved out of the northern PRVI margin (Figure 3). This study focuses on the larger, westernmost headscarp that is 55-km wide, 6.1-km deep and extends to the base of the slope. The crown of the scarp incises the 2600 m contour and the base of the scarp is at the Marginal Basin at a water depth of the 6100 m. The average scarp height is approximately 3500 m (Figure 4a). The total seafloor area bounded by the amphitheater is equal to 1441 km^2 (Table 2).

On the basis of widely spaced SCS reflection data, earlier studies suggested that the submarine landslides associated with the amphitheaters involved only the removal of the uppermost carbonate strata (a limit of thickness of 1.6 km) (Schwab et al., 1991). The closely spaced EW96-05 SCS profiles extending over the scarp show offsets in volcaniclastic basement reflectors which suggests that the slide plane in some locations extends up to 2 km below the seafloor into the Cretaceous to Lower Oligocene volcanic and sedimentary rocks underlying the Lower Pliocene to Lower Oligocene carbonate cap (Figure 5). A band of undulating, moderate amplitude reflectors of the rock unit beneath the carbonate platform strata are correlated to fluvial deposits of the San Sebastian Formation (Figure 5; SCS line 19). The San Sebastian Formation is well exposed onland in Puerto Rico and includes coal seams, shale intervals, and poorly consolidated sandstone units that are likely to form an unstable substrate facilitating the failure of the more massive, overlying carbonate units (Monroe, 1980).

Submarine Landslide Deposits

Submarine landslide deposits associated with the amphitheater extend up to 80 km north of the amphitheater crown, covering a total seafloor area of 4313 km^2 (Figure 6). The deposits can be divided into several general morphologies: relatively intact slumps/rafted carbonate blocks on the headscarp slope, debris flows, and turbidites (Figure 6). The slumps and rafted blocks are imaged by the sidescan sonar as lens-shaped or rounded areas of low backscatter surrounded by a halo of higher return (Figures 4 b, c and 7). The debris flows are recorded on the sidescan sonar as downslope trending streams of higher reflectivity on the face of the headscarp (Figures 4b, c and 7). The streams of coarse-grained, disorganized, and highly reflective slope/shelf material are channeled downslope around the more cohesive, slump/slide portions of platform material (Figures 4 b,c and 7). Light gray, areas of homogeneous reflectivity on the distal Elevated Plain and Main Plain areas are interpreted to be seafloor covered by relatively fine-grain turbidites, hemipelagics, and pelagics (Figure 4 b, c)

EW96-05 SCS profile 20 shows that the high-reflectivity, downslope-trending streams of debris material observed in the sidescan sonar imagery correlate with hummocky subsurface reflections in areas proximal to the amphitheater headwall (Figures 4c, 5, 7). Hummocky reflections are interpreted as small, blocky debris (less than a few 10's of meters) mixed with shelf/upper-slope carbonate and terrigenous material. EW96-05 SCS profile 19 shows that an ~ 8-km long and 500-m thick block of the carbonate platform appears to have detached from the amphitheater margin along a northward dipping glide plane (Figure 8).

Downslope-trending debris flows of high reflectivity gradually change to a lighter, more homogeneous backscatter signature north of the base of the slope, extending toward the distal

areas of seafloor covered by submarine landslide debris (Figure 4 b, c). The change in reflectivity observed in the sidescan backscatter is interpreted as the area of seafloor covered by pelagics and turbidites.

Small-scale (up to 5-km long and less than 1-km wide) slope-parallel, linear sediment ridges on the seafloor at the base of the slope are imaged by the sidescan sonar (Figure 4 b, c). These seafloor features are similar to surface features of the Saharan debris flow documented by Masson et al. (1993). Their formation suggests that downslope resedimentation has occurred in more than one pulse.

The SCS profiles over the debris field, northward of the scarp, reveal that sub-surface reflections change from hummocky to stacked packages of well-stratified sediment towards the base of the slope and onto the Elevated Plain, the most distal area of seafloor detected to be covered by submarine landslide debris (Figures 4b, c, 5, & 6). EW96-05 SCS profile 20 images up to eight units interpreted as widespread, distal turbidite deposits on the Elevated Plain, some of which have been back-tilted against the southeastern flank of the Median Ridge (Figure 9). The individual packages of sediment range in thickness from 175 – 250 m forming a combined sediment thickness of 1600 m on the Elevated Plain.

A single, large debris flow can be traced as a continuous unit in the SCS profiles, up to 60 km north to its deposition on the Elevated Plain (Figures 5 & 9). The sediment package is acoustically unstratified and characterized by a smooth and strongly reflective basal surface. EW96-05 profile 20 shows deposition of at least four packages of sediment characterized by weakly reflective, parallel-subparallel subunits on top of the large debris flow unit (Figure 9). These later deposits mask the toe of the large debris unit, making it undetectable in the sidescan

sonar imagery and bathymetry.

Cores containing up to 8 m of the uppermost sediment in the Puerto Rico trench document three to four, coarse sand to lutite turbidite deposits on the Elevated Plain that are correlated with deposits in the main trench axis (Doull, 1984; Pilkey and Cleary, 1985) (Table 1). These deposits are much smaller (order of cms in thickness) than the eight events described above; consequently, the deposits are unresolveable by the SCS system. The shallow seafloor penetration of the cores would place the sandy turbidites within the uppermost unit on the seismic profiles (Figure 9).

Crescentic-Shaped Cracks

Large (~ 30 to 40 km long), crescentic-shaped cracks are discovered along the northwestern PRVI margin (Figures 4b and 10). These cracks in the PRVI carbonate platform are remarkably similar in both shape and length of the amphitheater-shaped headscarp, less than 40 km (measured from headscarp mid-point to mid-point) to the east. The most prominent of these features is a ~ 30 km long, E-SE trending crescentic-shaped headscarp (Figures 4b and 10). EW96-05 SCS profile 23 shows that along the approximately 200-m high escarpment, a 750-m thick section of the carbonate platform has begun to slump trenchward (Figures 11 & 12). The surficial area of the carbonate slump is roughly 500 km^2, equivalent to an approximate volume of 375 km^3 (Figure 6). In 1943, a magnitude 7.8 earthquake measured by Dolan and Wald (1998) occurred slightly northeast of the crescentic-shaped headscarp.

An approximately 40-km long, NE-SW trending crescentic-shaped crack is identified 20 km offshore northwestern Puerto Rico on the eastern flank of the Mona rift (Figures 4b and 10). The long crack appears to be the culmination of several small, *en echelon*, crescentic cracks

(Figures 4b and 10). EW96-05 SCS profile 23 shows that in many cases these cracks are normal faults that extend through the carbonate platform (Figures 11 & 13). Thus, these faults may serve as planes of weakness for future submarine landsliding of the PRVI carbonate material and underlying volcaniclastics. In this area, debris could potentially flow northward toward the trench or to the west into the deep waters of the N-S trending Mona Rift.

Mona Block

In the northwestern region of the EW9605 survey area, a section of the PRVI carbonate platform extends on top of an anomalous shallow (1000 mbsl) section of the upper slope, called the Mona Block (Figure 4). The "carbonate cap" is recognizable on the sidescan record as a narrow elongate region of high reflectivity (Figure 4 c, b). In EW96-05 SCS profile 26, the carbonate cap is seen as continuous, parallel reflectors (Figure 14). The sidescan sonar shows narrow, downslope-trending zones of both high and low reflectivity. This pattern is interpreted as very coarse to blocky streams of carbonate debris (Figure 4 b, c). The sidescan shows that the debris is channeled into the Mona rift and northward onto the Main Plain. On EW96-05 SCS profile 26, a northward dipping scarp is imaged. At its base is a 500 m thick unit of chaotic reflectors interpreted to be submarine landslide debris associated with the headscarp (Figure 14). It is believed that the Mona Block represents the upthrust section of the slope overlying the subducted southeastern tip of the Bahamas Province (Dolan et al., 1998; Grindlay et al., 2004).

Shelf Canyons and Headless Gullies

The PRVI carbonate platform is incised by narrow (less than 1 km wide) V or U-shaped features that are interpreted as shelf canyons that probably formed during times of lower sea

level. The canyons are characterized by narrow, sinuous, bands of high reflectivity that extend northward to the edge of the PRVI carbonate platform (Figure 7). They are inferred to serve as conduits for the transport of terrigenous sediments derived from river systems of northern Puerto Rico to the deeper waters of the trench. A number of the submarine canyons continue northward and incise the face of the amphitheater. These canyons are typically associated with what are interpreted to be debris flow deposits on the face of the headscarp. The relation between mass wasting and submarine canyons has been investigated by Hampton (1972). Hampton (1972) documented that mass wasting initiating in a canyon head, triggered by some mechanism, leads to the downslope movement of a debris flow. In one model, Hampton (1972) showed that continual downslope movement of the debris flows led to their evolution into more fluid turbidites. The idea that the landslide deposits along the northern margin of the PRVI show a transition from the morphology of debris flow to more stratified turbidite deposits is supported by this model (Figure 5 and 6).

The upper section of the amphitheater-shaped scarp is heavily eroded by headless gullies (Figure 7). The crescentic-shaped headscarp is gullied as well, although not to the extent of the amphitheater (Figures 4 and 7). The westward decrease in gullying suggests that mass wasting of the PRVI carbonate platform may be progressing westward. Thus the large amphitheater which is heavily eroded by the gullies, may be considered to be older than the less gullied cresentic scarp to the west.

The occurrence of the headless gullies along the amphitheater scarp is most likely not associated with shelf-slope sedimentation. In fact, their existence advocates some other causative mechanism. The northward-dipping carbonate platform contains an aquifer under artesian

pressure (Rodriguez-Martinez, 1995). These artesian conditions may drive fluid expulsion and the associated gullying along the headscarp margin (cf. Monterey Bay, Orange et al., 1999). Gullying along the headscarp could contribute to additional headward erosion and submarine landslides initiated along the amphitheater margin.

DISCUSSION

Area and Volume Calculations of the Amphitheater and Associated Landslide Deposits

Digital terrain models assembled from swath bathymetry and digitized EW9605 SCS reflection profiles 3, 19, 20, and 21 were used to calculate the area of the amphitheater and the seafloor affected by the debris field, and the volume of the indentation and debris deposit (Table 2). Constraints on the submarine landslide dimensions allows for the comparison of the northern Puerto Rico slope failure to other well-documented submarine landslides as well as providing input for future tsunamigenic submarine landslide modeling.

The two-dimensional surfaces that were generated and used to calculate the volume of material involved in the submarine landslide are the reconstructed slope bathymetry (S1) based on the contours of adjacent, intact slope, the present seafloor topography, post-landsliding (S2), and the base of the submarine landslide deposit (S3) (Figure 15).

An isopach map of the submarine landslide deposit was generated by subtracting the base of the submarine landslide deposit (S3) from the present seafloor topography (S2). Assuming a seismic velocity value of 1.8 km/s, an isopach map of the debris field shows that the amphitheater landslide deposit has a maximum thickness of 2850 m at the base of the slope. The debris field generally thins northward to a thickness of 350 m (Figure 15). A volume of 2572 km^3 for the submarine landslide was calculated by summing the volumes of 300-m thick slices of the deposit (Refer to Appendices A and B for details of the volume calculations). This method takes into account variation in the bathymetry of the landslide. Other volume calculation methods assume a constant thickness for the landslide deposit that often leads to an over-estimate of the actual debris volume (Urgeles et al., 1999; Wynn and Masson, 2003).

Determining the accurate volume for submarine landslides is difficult and error may have been introduced in the final volume calculation due to inaccuracy in the seismic velocities, landslide area contours and debris field extent, assumed seismic reflection picking, the simplified reconstruction of the slope prior to the submarine landslide event, and porosity estimates. To account for these uncertainties, a 20% error margin was applied and a gross volume of the landslide deposit of 2572 +/- 514 km^3 was obtained (Table 2).

Comparison of Volume of Void and Volume of Submarine Landslide Debris

The landslide deposits and the *in situ* PRVI margin sedimentary and volcaniclastic rocks vary in porosity. Thus, a legitimate comparison of the negative volume of the voided amphitheater with the positive value of the submarine landslide debris needs to take into account the compaction factors of both the margin rock and submarine landslide material. An average porosity of 15% is used for the PRVI margin rocks based upon well data of the carbonate platform and underlying volcaniclastics basement rocks (Anderson, 1991). An assumed porosity of 50% for the landslide deposit is based on the measured porosities of debris flows and turbidites offshore Baja California (Moore et al., 1982), Bahamas Banks (Eberli, 1988; Williams et al., 1988), and the Middle America accretionary margin (Taylor and Fisher, 1993) (Table 3). In view of the similarities in compositions and grain size to the debris flows in this study, this value is considered a good first-order approximation. Mass conservation implies that the volume of the voided slope-forming margin rock should be equal to that of the submarine landslide deposit. The mass balance equation that we use is adapted from Collot et al. (2001):

$$(V1 * C1) - (V2 * C2) = 0$$

where V1 represents the volume of the amphitheater-shaped void and V2 represents the gross

volume of the submarine landslide deposit. C1 and C2 represent the compaction factors for the PRVI margin rocks and the debris flow deposits, respectively.

Applying the compaction factors for each 300-m thick slice of the landslide deposit gives a gross, compacted submarine landslide volume of 1426 km^3 +/- 285 km^3. This value is comparable to the 1378 +/- 275 km^3 compacted volume calculated for the amphitheater indentation. It is therefore possible that the entire submarine landslide deposit could be associated with mass wasting of the northern PRVI slope now bounded by the amphitheater. The calculated volume is similar to known tsunamigenic submarine landslides. For a comparison, one of the documented Storegga submarine landslides off the coast of Norway had a similar volume of 1700 km (Table 4). The Storegga slide generated a tsunami that affected the coast of Scotland 25 to 30 m above sea level (Dawson and Smith, 2000).

Since submarine landslides are rarely witnessed, it becomes difficult to determine if they typically occur as a single, catastrophic event or as multiple small events. Wynn and Masson (2003) have documented stacked turbidite deposits associated with the Canary Islands submarine landslides that they infer to be multiple stages of landslide failure. On the basis of their findings, Wynn and Masson (2003) argue that assuming submarine landslide occurs as one event potentially oversimplifies the failure process. In many cases this oversimplification will lead to overestimates of submarine landslide volumes and run up estimates calculated in corollary tsunami wave models. The stacked and correlateable units that are imaged by the SCS profiles on the Elevated Plain of the northern PRVI margin suggest that landsliding associated with the amphitheater is more complex than just one event. It is therefore likely that the landslide volumes calculated in this paper represent the summation of multiple landslide events initiated

along the amphitheater over time. Nevertheless, even small volume submarine landslide events (less than 10's of km) are capable of generating a tsunami and therefore warrant study. For example, a wave height of 15 m was recorded for the 1998 Papua New Guinea tsunami which was generated by a submarine landslide only ~ 6 km^3 in volume (Tappin 1999; Synolakis et al., 2002).

Triggering Mechanisms for Submarine Landslides on the Northern PRVI Margin

The neotectonic setting of the northern PRVI margin supports a multitude of processes capable of initiating submarine landslides. Perhaps one of the most significant contributors to a loss of seafloor shear strength and the initiation of a catastrophic submarine landslide is frequent and intense episodes of seismic shaking. Mullins et al., (1992) have interpreted similar large, amphitheater-shaped "scallops" along the southeast Bahamas-Hispaniola collision zone to be catastrophic collapses structures triggered by large magnitude earthquakes. Earthquakes of large magnitude occurring along the North America-Caribbean plate interface thrust zone, along one of the forearc strike-slip faults, or in the Mona Block region could elevate sediment pore-water pressure and lead to catastrophic landsliding of seafloor material. Poor downhole recovery of the cores used in this study limits their use for detailed age-dating of submarine landslide deposits to link them to past seismic events. Future studies that include high-resolution coring of targeted submarine landslide deposits have the potential to allow correlation with onland studies addressing prehistoric seismicity in the region (Prentice and Mann, 2004; Tuttle et al, 2004).

The crescentic shape of the headscarps along the northern slope of Puerto Rico is considered to be the "beginning of the end" of carbonate platform margins (Mullins and Hine 1989). Mullins and Hine hypothesize that these amphitheater-shaped headscarps are largely

erosional features that represent collapse of the margin. Once failure is initiated, mechanisms such as chemical dissolution, fluid explusion, bioerosion, and turbidity currents promote headward erosion of the scarp and progressive carbonate platform collapse. The system of headless gullies imaged by the sidescan sonar along the amphitheater head scarp suggest that groundwater seeps are present along the northern PRVI margin. Definitive tests for submarine discharge, such as water and rock sampling and visual inspection, however, have yet to be conducted. Higher resolution sidescan sonar imagery is needed upslope of the headscarp to verify the presence of coalescing cracks that are indicative of headward erosion.

The present-day collision zone of the southeastern tip of the Bahamas Province is thought to be offshore northwest Puerto Rico (Dolan et al., 1998; Grindlay et al., 2004). The uplifted Mona Block and associated debris flows and the crescentic cracks in the carbonate platform on the eastern flank of the Mona Rift are thought to be manifestations of upper-plate deformation associated with the subduction of the high-standing SE Bahamas. The association of seamount subduction with enhanced forearc deformation and erosion has been well documented along other convergent margins. For example, a 55-km wide slump along the Pacific coast of Costa Rica at the Cocos-Caribbean plate convergent margin resulted from slope oversteepening due to the underthrusting of a seamount on the subducting plate (von Huene and Ranero, 2001). Collot et al. (2001) provide convincing evidence that the Ruatoria debris avalanche (~ 3000 km^3) off the coast of New Zealand was the result of the subduction of a seamount which left steep slopes susceptible to failure in its wake. The concentric cracks are reminiscent of cracks seen in physical models of upper-plate deformation associated with the oblique subduction of seamounts by Dominguez et al. (1998a) and observed along other active margins where seamount

subduction is suspected (e.g. Ryukyu margin, Dominguez et al., 1998; central Chile forearc, Laursen and Normark, 2002) (Figure 16).

Implications for Tsunamigenesis

The EW96-05 survey has revealed sites where potential future submarine landslides may occur along the northern PRVI margin. The proximity of the crescentic cracks to the tectonically active Mona Rift make them likely candidates for sites of future seismically triggered, large-scale submarine landslides. McCann and Mercado (1998) speculate that the 1918 tsunami was the result of seafloor rupture thought to occur along the N-S trending Mona Canyon fault, that lies slightly southwest of the crescentic-shaped seafloor cracks (Figure 4). However, given evidence of multiple submarine landslide deposits adjacent to Mona Block and within the Mona Rift, the tsunami that inundated western Puerto Rico could have also been generated by a submarine landslide event that was triggered by the large magnitude earthquake.

Although the magnitude of the tsunami generated by a submarine landslide is determined by many factors, the most important consideration is the amount of seafloor deformation and subsequent water displacement (Ward, 2001). Lynett and Lui (2003) modeled the tsunami that would have been generated if the amphitheater-shaped scarp was remnant of a single landslide event. Lynett and Lui (2003) applied a wave model equation that integrated variation in seafloor depth. Assuming that the submarine landslide occurred as a catastrophic, northward rotational slump of 900 km^3 – 1000^3 km sediment, Lynett and Lui, (2003) modeled a wave with run up heights of up to 70 m along the north coast of Puerto Rico about 15 minutes after the initiation of slope failure. Impact would have been the greatest among the larger of the north coast cities that

include the island's capital of San Juan (approx. population of 437,900) and Arecibo (approx. population of 51,200) (United States Census Bureau, 2004).

The 1378 km^3 volume bound by the amphitheater calculated in this paper is nearly one-third greater than the 900 km^3 value that Lynett and Lui (2003) used for their wave modeling. Assuming all other factors remained the same, if the 1378 km^3 value were used in the wave equation, run up values would presumably be much greater. Moreover, assuming a uniform carbonate platform thickness of 1.6 km and surface area of 500 km^2, a submarine landslide along the crescentic-shaped cracks on the eastern flank of the Mona Rift could represent the removal of up to 400 km^3 of PRVI margin rock. This volume is approximately one-third the value used by Lynnet and Lui (2003) in their models. Although, wave run up due to catastrophic submarine landsliding at here would likely be significantly less than that calculated for the amphitheater, run ups of a even few meters represents a significant hazard to the low-lying and densely populated coastal areas of northwestern Puerto Rico.

CONCLUSIONS

The systematic EW96-05 marine geophysical survey over the northern PRVI margin and Puerto Rico trench region allowed for generation of the highest-resolution map of the seafloor surface and subsurface in this area. On the basis of the morphological and structural analysis of these data, the following conclusions were reached:

1. The northern PRVI margin is characterized an extensive submarine landslide deposits that cover a total seafloor area of 4313 km^2 and can be traced 80 km up-slope to a 55-km wide amphitheater-shaped headscarp. An isopach map of the area shows that the maximum thickness of the deposit reaches 2850 m and has a total compacted volume of 1426 km^3. The seismic reflection data show that in many localities, the deposit is characterized by multiple, parallel units ranging in thickness from 175 m – 250 m.
2. The compacted volume of PRVI margin rock associated with the amphitheater is calculated to be 1378 km^3 , and the compacted volume of the submarine landslide debris field is 1426 km^3. The similar results in volume show that the mapped debris field could be associated with the formation of the giant amphitheater. The most likely scenario for the formation of the amphitheater is that submarine landsliding is complex and that the stacked turbidite sequences are representative of multiple submarine landslide events initiated along the slope of the amphitheater. Unlike other convergent margins, the submarine landslide deposits do not seem to have been transported elsewhere or subducted.
3. The northern PRVI margin supports a multitude of processes capable of initiating submarine landslides. Although the exact cause of failure that generated the large

amphitheater is not known, it is most likely the result of a combination of processes that are related to the subduction of the SE Bahamas beneath the margin. The westward migration of the overthickened SE Bahamas has resulted in rapid subsidence, slope oversteepening, and collapse of the margin since the Neogene (Grindlay et al., 2004).

4. The discovery of the large (~ 35-40-km long) crescentic-shaped headscarp and crescentic-shaped cracks on the eastern flank of the Mona Rift illustrate locations for future submarine landslides of the PRVI carbonate platform. Given their close proximately to the tectonically active Mona rift, catastrophic submarine landslides along these seafloor features is possible.
5. Based on the comparisons with other well-documented tsunamigenic submarine landslides and preliminary tsunami wave modeling (Lynette and Lui, 2003), the northern PRVI submarine landslide that generated the amphitheater was most likely tsunamigenic. The discovery of submarine landslide deposits offshore northwestern Puerto Rico suggests that the 1918 tsunami event could have been caused by a submarine landslide.

REFERENCES

Anderson, R. N., 1991. Geophysical logs from the Toa Baja scientific drillhole, Puerto Rico. Geophysical Research Letters 18, 497-500.

Bowin, C., 1972. Puerto Rico trench negative anomaly belt, GSA Mem. 132, 339-350.

Calais, E., Mercier, B., 2002. From transpression to transpression along the northern Caribbean plate boundary: implications for recent motion in the Caribbean plate , Tectonophysics 186, 329-350.

Collot, J-Y., Lewis, K., Lamarche, G., Lallemand, S., 2001. The giant Ruatoria debris avalanche on the northern Hikurangi margin, New Zealand: Result of oblique seamount subduction. Journal of Geophysical Research 106 (B9), 19271-19297.

Connolly, F., Ewing, M., 1967. Sedimentation in the Puerto Rico Trench, Journal of Sedimentary Petrology 37, 44-59.

Cruden, D.M. and Varnes, D.J., 1996. Landslide types and processes: *in* Turner, A.K. and Schuster, R.L., Landslides - Investigation and Mitigation, Transportation Research Board Special Report 247, 6-75.

Dawson, S., Smith, D.E., 2000. The sedimentology of Middle Holocene tsunami facies in northern Sutherland, Scotland, UK. Marine Geology 170, 69-79.

Dillon, W.P., Edgar, T., Scanlon, K.M., Coleman, 1996. A review of the tectonic problems of the strike-slip northern boundary of the Caribbean Plate and examination by GLORIA, in: Garder. J.V., Field, M.E., Twitchell, D.C., (Eds.), Geology of the United States' Seafloor: The View from GLORIA, Cambridge University Press, Cambirdge, U.K., 135 – 164.

Dingle, R.V., 1977. "The anatomy of a large submarine slump on a sheared continental margin (southeast Africa), " Journ. Geol. Soc. London 1354, 293-310.

Dolan, J.F., Mullins, H.T., Wald, D.J., 1998. Active tectonics of the north central Caribbean: Oblique collision, strain partitioning, and opposing subducted slabs, in: Dolan, J.F., Mann, P., (Eds.), Active Strike-Slip and Collisional Tectonics of the Northern Caribbean Plate Boundary Zone, Spec. Paper Geological Soc. Amer., 326, 1-61.

Dominquez, S., Lallemand, S., Malavielle, J., Schnurle, P., 1998. Oblique subduction of the Gagua Ridge beneath the Ryukyu accretionary wedge system: Insights from marine observation and sandbox experiments, Marine Geophysical Researches 20, 383-402.

Doull, M. 1984. Turbidite Deposits in the Puerto Rico Trench Abyssal Plain. unpublished Master's thesis, Duke University, 124 pp.

Eberli, G.P., 1988. Physical properties of carbonate turbidite sequences surrounding the Bahamas – Implications for slope stability and fluid movements, Proceedings of the Ocean Drilling program, Scientific Results 101, 305-314.

Embley, R.W., 1982, Anatomy of some Atlantic-margin sediment slides and some comments on ages and mechanisms. in: Saxov, S., Nieuwenhuis, J.K., (Eds.), Marine Slides and Other Mass Movements, Plenum: NY, p. 189-214.

Embley, R.W., Jacobi, R., 1986. Mass wasting in the western North Atlantic, in: Vogt, P.R., Tucholke B.E., (Eds.), The Geology of North America , Volume M, The Western North Atlantic Region, Geological Society of America, p. 479-490.

Grindlay, N.R., N.R., Mann, P., Dolan, J.F., van Gestel, J-P, 2004. Neotectonics and subsidence of the northern Puerto Rico-Virgin Islands margin in response to oblique subduction of high-standing ridges, in: Mann, P. (Ed.), Active tectonics and seismic hazards of Puerto Rico, the Virgin Islands, and offshore areas. Geological Society Special Paper, accepted.

Hampton, M.A., 1972. The role of subaqueous debris flow in generating turbidity currents, Journal of Sedimentary Petrology 42, 775-793.

Hampton, M., Lee, H., Locat, J., 1996. Submarine landslides, Reviews of Geophysics 34, 33-59.

Heezen, B.C., Ewing, M., 1952. Turbidity currents and submarine slumps and the 1929 Grand Banks earthquake, American Journal of Science 250, 847-873.

Jansma, P.E., Lopez, A., Mattioli, G.S., DeMets, C., Dixon, T.H., Mann, P., Calais, E., 2000. Neotectonics of Puerto Rico and the Virgin Islands, northeastern Caribbean from GPS geodesy. Tectonics 9, 1021-1037.

Jiang, L., LeBlond, P.H., 1992. The coupling of a submarine slide and the surface waves which it generates, Journal of Geophysical Research 97 (C8), 12731-12744.

Laursen, J., Normark, W.R., 2002. Late Quaternary evolution of the San Antonio Submarine Canyon in the Central Chile forearc (~ 33° S), Marine Geology 188, 365-390.

Larue, D.K., Ryan, H.F., 1998. Seismic reflection profiles of the Puerto Rico Trench: Shortening between the North American and Caribbean plates, in: Lidiak, E.G., Larue, D.K. (Eds.), Tectonics and Geochemistry of the Northeastern Caribbean. Geological Society of America, Special Paper 322, 193-210.

Lastras, G., Canals, M., Hughes-Clarke, J.E., Moreno, A., De Batist, M., Masson, D.G., Cochonat, P., 2002. Seafloor imagery from the BIG ’95 debris flow, western Mediterranean, Geology 30, no, 10, 871-874.

Lee, H.J., Schwab, W.C., Booth, J.S., 2002. Submarine landslides: An Introduction, in: Schwab,

W.C., Lee, H.J., and Twichell, D.C., (Eds.), Submarine Landslides Selected Studies in the U.S. Exclusive Economic Zone, U.S. Geological Survey Special Bulletin, 2002.

Locat, J., and Lee, H.J., 2002. Submarine landslides: advances and challenges. Canadian Geotechnical Journal 39, 193-212.

Lynett, P., and Lui, P. L.-F., 2003. Submarine landslide generated waves modeled using depth-integrated equations, in: Yalciner, A.C., Pelinovsky, E.N., Okal, E., Synolakis, C.E. (Eds.), Submarine Landslides and Tsunamis: Kluwer Academic Publishers, NATO Science Series, vol. 21.

Mann, P., Calais, E., Ruegg, J-C., DeMets, C., Jansma, P.E., Mattioli, G.S., 2002. Oblique collision in the northeastern Caribbean from GPS measurements and geological observations. Tectonics 21 no. 6, 1-25.

Masson, D.G., Huggett, Q.J., Brunsden, D., 1993. The surface texture of the Saharan Debris Flow deposit and some speculations on submarine debris flow processes, Sedimentology 40, 583-598.

Masson, D.G., Kenyon, N.H., Weaver, P.P.E., 1998. Slides, Debris Flows, and Turbidity Currents, in: Summerhayes, C.P., S.A. Thorpe (Eds.), Oceanography: An Illustrated Guide, Kluwer Academic Publishers: New York, pp. 136-151.

McAdoo, B. G., 1999. Mapping Submarine Slope Failures, in: Wright, D., Bartlett, D., (Eds.), Marine and Coastal Geographic Information Systems, Taylor and Francis, Publishers, New York, p. 179-204.

McCann, W.R., and Sykes, L., 1984. Subduction of aseismic ridges beneath the Caribbean plate: Implications for the tectonics and seismic potential of the Northeastern Caribbean, Journal of Geophysical Research 89, 4493-4519.

McCann, W.R., 1985. On the earthquake hazards of Puerto Rico and the Virgin Islands. Bulletin of the Seismological Society of America 75 no. 1, 251-262.

McCann, W.R., 2002. Microearthquake Data Elucidate Details of Caribbean Subduction Zone. Seismological Research Letters 73, no. 1, 25-32.

Mercado, A., and McCann, W., 1998. Numerical simulation of the 1918 Puerto Rico tsunami. Journal of Natural Hazards 18, 57-76.

Meyerhoff., H.A., Krieg, E.A., Cloos, J.D., Taner, I., 1983. Petroleum potential of Puerto Rico, Oil and Gas Journal 81, 113-120.

Monroe, W.H., 1980. Geology of the middle Tertiary formations of Puerto Rico, U.S. Geological Survey Professional Paper, pp.953-93.

Moore, D.G., Curray, J.R., Einsele, G., 1982. Salado-Vinorama submarine slide and turbidity current off the SE tip of Baja California, Initial Reports of the Deep Sea Drilling Project 64, 1071-1082.

Moore, J.G., Clague, D.A., Holcomb, R.T., Lipman, P.W., Normark, W.R., Torresan, M.E., 1989. Prodigious submarine slides on the Hawaiian Ridge, Journal of Geophysical Research 94, 17465-17484.

Morgenstern, N.R., 1967. Submarine slumping and the initiation of turbidity currents, in: Richards, A.F. (Ed.), Marine Geotechinque: University of Illinois Press, Urbana, IL, pp. 189-220.

Moussa, M.T., Seiglie, G.A., Meyerhoff, A.A., Taner, I., 1987. The Quebradillas Limestone (Miocene-Pliocene), northern Puerto Rico, and tectonics of the northeastern Caribbean margin. Geological Society of America Bulletin 99, 427-439.

Mullins, H.T., Breen, N., Dolan, J., Wellner, R.W., Petruccione, M.G., Andersen, B., Melillo, A.J., Jurgens, A.D., Orange, D., 1992. Carbonate platforms along the southeast Bahamas-Hispaniola collision zone. Marine Geology 105, 169-209.

Orange, D., Greene, H., Reed, D., Martin, J., McHugh, C., Ryan, W., Maher, N., Stakes, D., Barry, J., 1999. Widespread fluid expulsion on a translational continental margin: Mud volcanoes, fault zones, headless canyons, and organic-rich substrate in Monterey Bay, California, GSA Bull. 11, 992-1009.

Pilkey, O. Cleary, W. 1985. Turbidite Sedimentation in the Puerto Rico Trench, in: Vogt, P.R., Tucholke B.E. (Eds.), The Geology of North America , Volume M, The Western North Atlantic Region: Geological Society of America, 437-450.

Prentice, C., and Mann, P., 2004. Paleoseismic Study of the South Lajas Fault, Lajas Valley, Southwestern Puerto Rico , in: Mann, P. (Ed.), Active tectonics and seismic hazards of Puerto Rico, the Virgin Islands, and offshore areas. Geological Society Special Paper, accepted.

Ranero, C.R., von Huene, R., 2000. Subduction erosion along the Middle America convergent margin, Nature 404, 748-752.

Reid, H., Taber, S., 1919. The Puerto Rico earthquakes of October-November 1918 Bulletin of the Seismological Society of America 9, 95-127.

Rodriguez-Martinez, J., 1995. Hydrogeology of the North Coast Limestone aquifer system of Puerto Rico, U.S. Geological Survey Water Resources Investigation Rpt. 94-4249, 22 pp.

Schwab, W.C., Danforth, W.W., Scanlon, K.M., Masson, D.G. 1991. A giant submarine slope failure along the northern insular slope of Puerto Rico. Marine Geology 96, 237-246.

Synolakis, C., Bardet, J-P., Borrero, J., Davies, H., Okal, E., Silver, E., Sweet, S., Tappin, D., 2002. The slump origin of the 1998 Papua New Guinea tsunami. Proc. R. Soc. London 457, 1-27.

Tappin, D.R., Matsumoto, T., Watts, P., Satake, K., McMurty, G.M., Matsuyama, M., Lafoy, Y., Tsuji, Y., Kanamatsu, T., Lus, W., Iwabuchi, Y., Yeh., H., Matumotu, Y., Nakamura, M., Mohoi, M., Hill, P., Crook, K., Anton, L., 1999. Sediment slump likely caused the 1998 Papua New Guinea tsunami. Eos. Transactions of the American Geophysical Union 80, 329-340.

Tappin, D.R., Okal, E., 2003. Dating Submarine Landslides: the July 17th 1998 Papua New Guinea Event Eos. Transactions of the American Geophysical Union 84 (46), Fall Meeting Abstract OS22A329-1147.

Taylor, E., Fisher, A., 1993. Sediment Permeability at the Nankai Accretionary Prism, Site 808, Initial Reports of the Deep Sea Drilling Project 131, 235-245.

Tuttle, T., 2004. Liquefaction Induced by Historic and Prehistoric Earthquakes in Puerto Rico, in: Mann, P. (Ed.), Active tectonics and seismic hazards of Puerto Rico, the Virgin Islands, and offshore areas. Geological Society Special Paper, accepted.

Urgeles, R., Masson, D.G., Canals, M., Watts, A.B., and Le Bas, T., 1999. Recurrent giant, submarine landslides on the west flank of La Palma, Canary Islands, Journal of Geophysical Research 104, 25331-25348.

Ward, S.N., 2001. Landslide tsunami, Journal of Geophysical Research 106, 11201-11215.

Westbrook, G.K., and McCann, W.R., 1986. Subduction of Atlantic lithosphere beneath the Caribbean, in: Vogt, P.R., Tucholke, B.E. (Eds.), The Geology of North America, Volume M, The Western North Atlantic Region: Geological Society of America.

Williams, C.F., Anderson, R.N., Austin, J.A.,Jr., 1988. Structure and evolution of the Bahamian deep-water channels: Insights from *in situ* geophysical and geochemical measurements, Proceedings of the Ocean Drilling Project 10439-451.

Wynn, R.B., Masson, D.G., (in press). Canary Islands landslides and tsunami generation, in: Locat, J., Mienert, J., (Eds.), First International Symposium on Submarine Mass Movements and Their Consequences. Kluwer Academic Publishers.

van Gestel, J., Mann, P., Dolan, J.F., Grindlay, N.R., 1998. Structure and tectonics of the upper Cenozoic Puerto Rico-Virgin Islands carbonate platform as determined from seismic reflection studies. Journal of Geophysical Research 103 (B12), 30505-30530.

van Gestel, J., Mann, P., Grindlay, N.R., Dolan, J.F., 1999. Three-phase tectonic evolution of the

northern margin of Puerto Rico as inferred from an integration of seismic reflection, well, and outcrop data. Marine Geology 161, 257-286.

Varnes, D.J., 1978. Slope Movement types and processes. In: Schuster, R.L., Krizek, R.J. (Eds.), Landslides – Analysis and Control: National Academy of Sciences Transportation Research Board Special Report No. 176, p. 12-33.

von Huene, R., Bourgois, J., Miller, J., Pautot, 1989. A large tsunamogenic slide and debris flow along the Peru Trench, Journal of Geophysical Research 94 (B2) 1703-1714.

von Huene, R., Ranero, C., 2001. Subduction erosion and basal friction along the sediment starved convergent margin of Antofagasta, Chile, Journal of Geophysical researches, Journal of Geophysical Researches 108, 2079-2084.

Table 1. Giant Elevated Plain Turbidite (EP-3)

Core	Lat, Long	Water depth (m)	Sand turbidite thickness (cm)	Sand size	Overlying turbidite thickness (cm)	Turbidite description	Basal age
PR21	19º 19'N, 66º 09.0' W	7929	418	v. fine to coarse	738	Distorted with lutite inclusions and limestone fragments	Pleist.
C9-40	19º 19.9'N, 66º 06.3'W	7921	176	fine to coarse	217	Eroded, core straightened lutite inclusions	Pleist.
PR22	19º 20.5'N, 66º 22.6' W	7929	139	v. fine to almost coarse	8	Full sequence with eroded basal and upper surfaces	Pleist.
PR23	19º 20.7' N, 66 32.6º W	7961	11	v. fine to fine	19	No description	Plio.
PR24	19º 29.1' N, 66º 36.6' W	7971	110	v. fine to medium	20	Full sequence, primarily mottled lutite	Plio. – Pleist.
PR25	19º 32.2' N, 66º 43.1' W	7950	6	fine to fine/med	20	Full sequence, primarily mottled lutite	Pleist.

Description of cores showing evidence of extensive turbidite deposits in the Elevated Plain at the base of the headscarp slope (Doull, 1984; Connolly and Ewing, 1967). Overlying the giant, Elevated Plain sand turbidite is a thick lutite-rich turbidite.

Table 2. Areas and Volumes Calculated for the Submarine Landslide and Amphitheater-shaped Scarp*

Region	**Name**	**Area (km^2)**	**Volume (km^3)**	**Error (20%) (km^3)**	***in situ* porosity (%)**	**Compact Volume (km^3)**	**Error (20%) (km^3)**
Amphitheater	V1	1441	1622	324	15	1378	275 (pre-failure)
Depth of crown (m)	2600 m						
Length of slope (m)	~ 3000 m						
Max scarp width (m)	~ 5500 m						
Total landslide	V2	4313	2572	514	50	1426	285
Runout length (m)	8400 m						
Max width (m)	5600 m						
Max thickness (m)	2850 m						
Min thickness (m)	350 m						
Diff. between pre- & post-landslide	V3		1915	383		48	

*Amphitheater and landslide regions are defined in figure 15. Numbers are rounded to the nearest integer. V1, V2, and V3 are defined in figure 15. Porosity values for the carbonate platform and debris flows from Eberli (1988), Williams et al. (1988), Moore et al. (1982), Anderson (1991), Taylor and Fisher (1993), and Moran et al. (1993. Landslide thickness was calculated using a p-wave velocity of 1800 m/s (Moore et al., 1982; Collot et al., 2001). Compacted Volume is equal to Volume x (100 – Porosity)/100. Compacted landslide volume for 300-m thick slices is calculated and shown in Table 3.

Table 3. Compaction of Landslide Deposit

Slices (m)	Volume (km^3)	P1 (%)	P2 (%)	Pav (%)	C2 (%)	Vcomp (km^3)
0-300	1095	20	65	56	44	481
300-600	613	18	44	41	59	361
600-900	326		38	38	62	202
900-1200	224		34	34	66	147
1200-1500	148		27	27	73	108
1500-1800	94		26	26	74	69
1800-2100	45		23	23	77	34
2100-2400	23		17	17	83	19
2400-2700	5		15	15	85	4
> 2700	1		12	12	88	0.8
Total	2572					1426

The submarine landslide isopach map is divided into 300-m thick slices in which the volume of the individual slices is calculated using grdvolume GMT 3.1. P1 is the porosity of slumps and blocks. P2 is a depth-dependant porosity of the debris flow and turbidite material (Eberli, 1988; Williams et al., 1988; Moore et al., 1982; Taylor and Fisher, 1993; Moran et al.; 1993). The submarine landslide debris field is estimated to consist of ~80% debris flows and turbidites and 20% slumps and blocks at a thickness of 0-300 m (Pav = 0.2*20+0.8*65). At 300-600 m the debris field consists of ~90% debris flows and turbidites and 10% slumps and blocks (Pav = 0.1*18+0.9*44). Beyond 600 m, the debris field is interpreted to consist of 100% debris flow and turbidite material (Pav = P2) (Eberli, 1988; Williams et al., 1988; Moore et al., 1982; Taylor and Fisher, 199). Slice compaction is defined as C2 = 100-Pav and the compacted volume of each slice is the original slice volume (km^3) multiplied by the slice compaction factor (C2)/100 (Collot et al., 2001).

Table 4. Approximate volumes of well-documented submarine landslides. Starred locations are documented to have had historical tsunamis. If slope failure along the northern PRVI margin occurred as a single submarine landslide, the event would have involved the catastrophic removal of approximately 1426 km^3 of compacted material. A more likely scenario is that the amphitheater was formed by multiple, smaller and still potentially tsunamigenic debris flows and turbidites.

Documented Submarine Landslides	**Approximate Volume (km^3)**
Nuuanu, Hawaii[1] *	5000
Ruatoria	3146
Canary Islands[1]	400
Storegga Slides, Norway[2] *	1700
PRVI northern margin	1426
Grand Banks 1929 turbidite[1] *	185
BIG '95, Mediterranean[3]	26
Saharan[1]	600
Papua New Guinea, 1998[4] *	6

([1]Masson et al., 1998; [2]Dawson and Smith, 2000; [3] Lastras et al., 2002; [4] Tappin and Okal, 2003).

Figure 1. Color shaded relief map of the NE Caribbean region showing regional plate boundaries and interactions. GPS plate motion vectors are relative to a fixed North America plate (Mann et al., 2002). Locations of the 1918 (Mw = 7.3) and 1867 (Mw = 7.5) earthquakes are shown (McCann, 1985). GPS stations: ISBA = La Isabel, Puerto Rico; ROJO = Cabo Rojo, Dominican Republic; SDOM = Santo Domingo, Dominican Republic; CAPO = Capotillo, Dominican Republic; TURK = Turk Island, Bahamas; FRAN = Cabo Frances Viejo; EPGFZ = Enriquillo-Plantain Garden fault; contours are at 500 m. Boxed area shows location of Figure 3. Inset shows location of study area relative to the S.E. United States, Central, and South America.

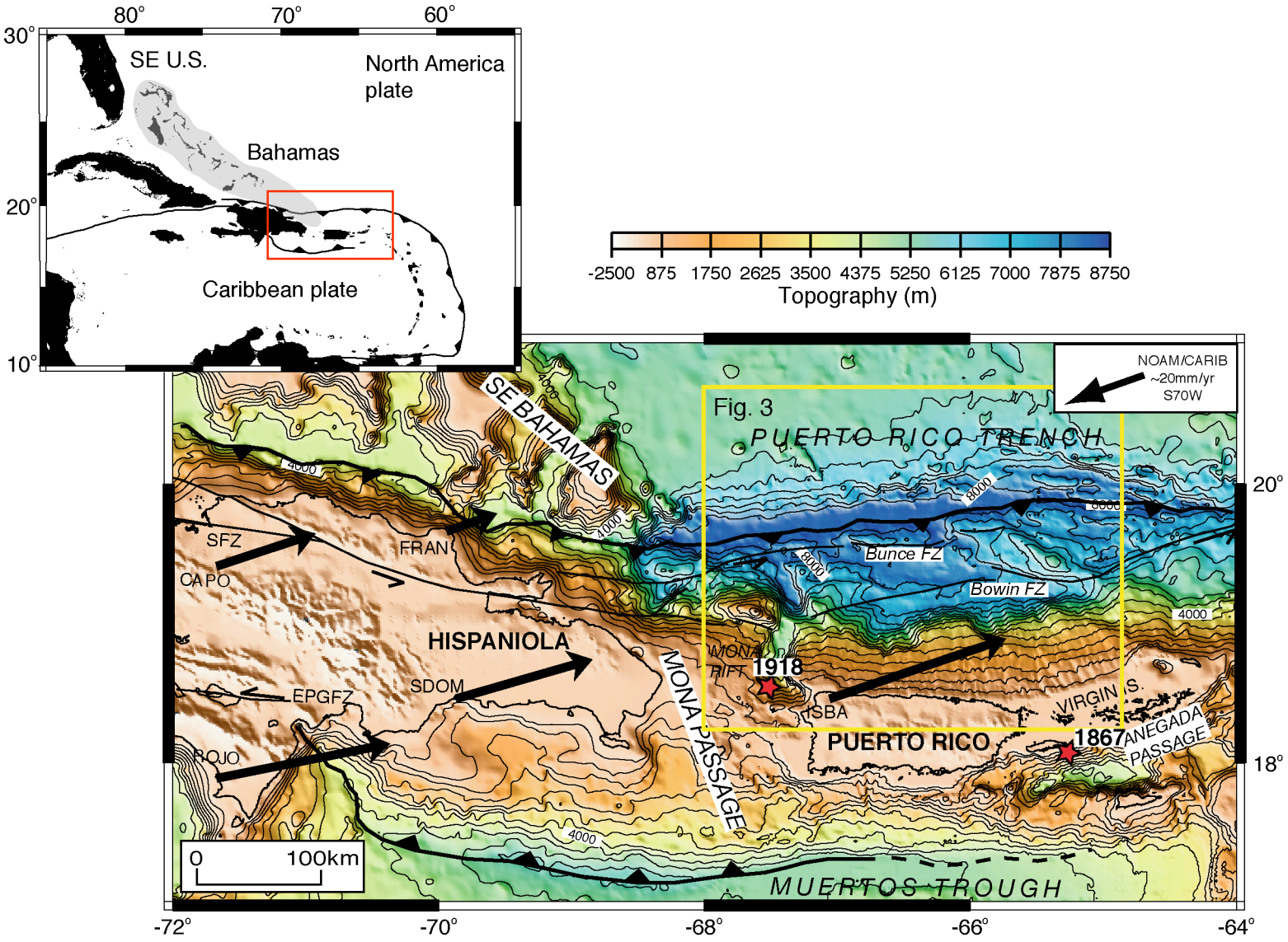
80°
70°
60°
30°
20°
10°
SE U.S.
North America plate
Bahamas
Caribbean plate
-2500 875 1750 2625 3500 4375 5250 6125 7000 7875 8750
Topography (m)
NOAM/CARIB
~20mm/yr
S70W
Fig. 3
PUERTO RICO TRENCH
SE BAHAMAS
SFZ
FRAN
CAPO
HISPANIOLA
SDOM
EPGFZ
ROJO
Bunce FZ
Bowin FZ
MONA RIFT
1918
ISBA
MONA PASSAGE
VIRGIN IS.
PUERTO RICO
1867
ANEGADA PASSAGE
MUERTOS TROUGH
0 100km
20°
18°
-72°
-70°
-68°
-66°
-64°

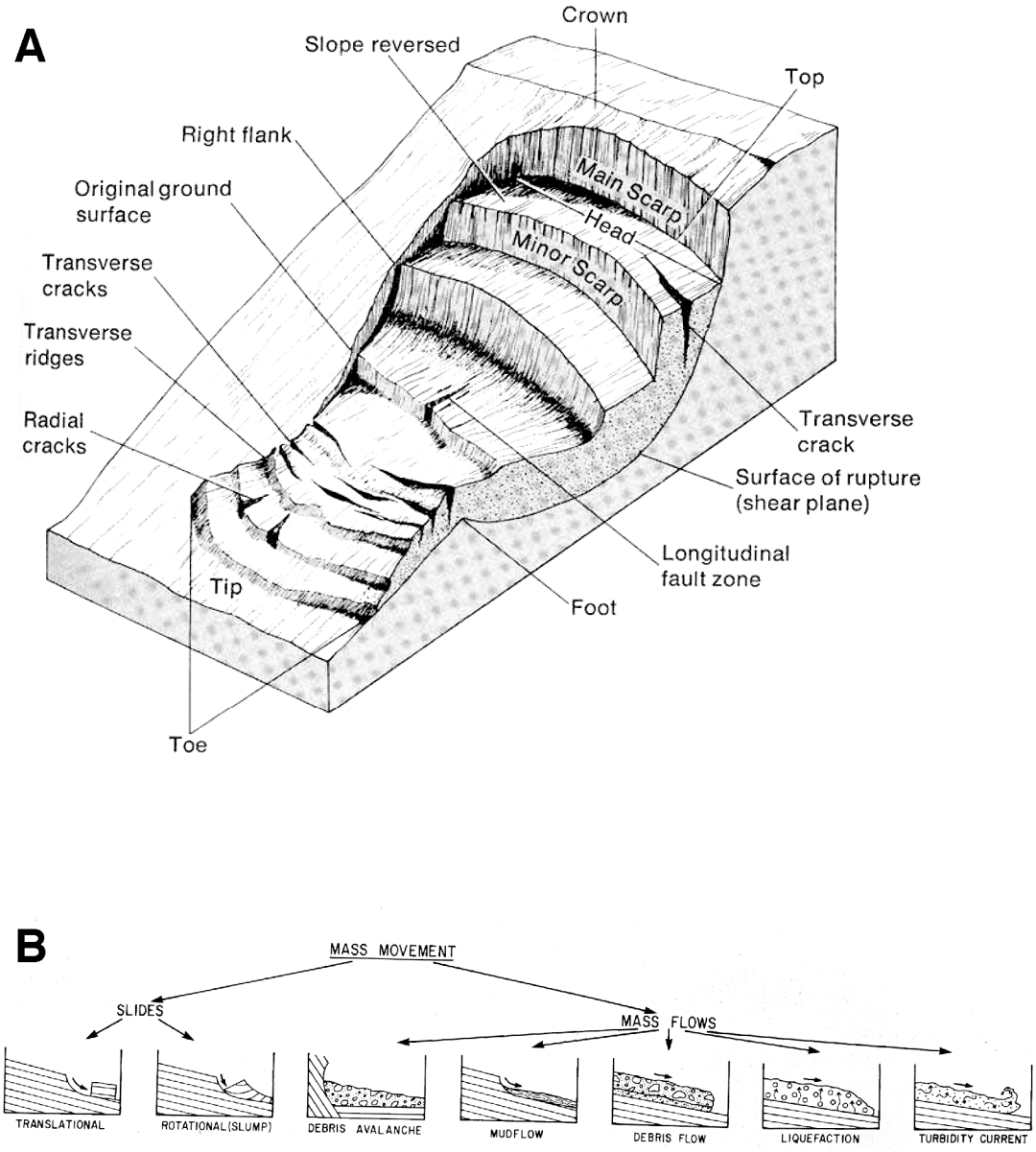

Figure 2. a) Landslide features and terminology from Varnes and Cruden (1996). b) Submarine landslide classification from Hampton (1972).

Figure 3. Hydrosweep bathymetric map of the study area showing major geologic seafloor features and bathymetry, contoured at every 200 m. ESFZ = East Septentrional fault zone. Thin black lines show the location of the EW96-05 cruise track lines. Thick lines identify the single-channel seismic reflection profiles used in this study. The updip extent of the carbonate platform on the island of Puerto Rico is shown by the black line. Shaded region off the north coast of Puerto Rico shows extent of seafloor covered by submarine landslide deposits. Boxed area shows the extent of the study area and location of Figure 4.

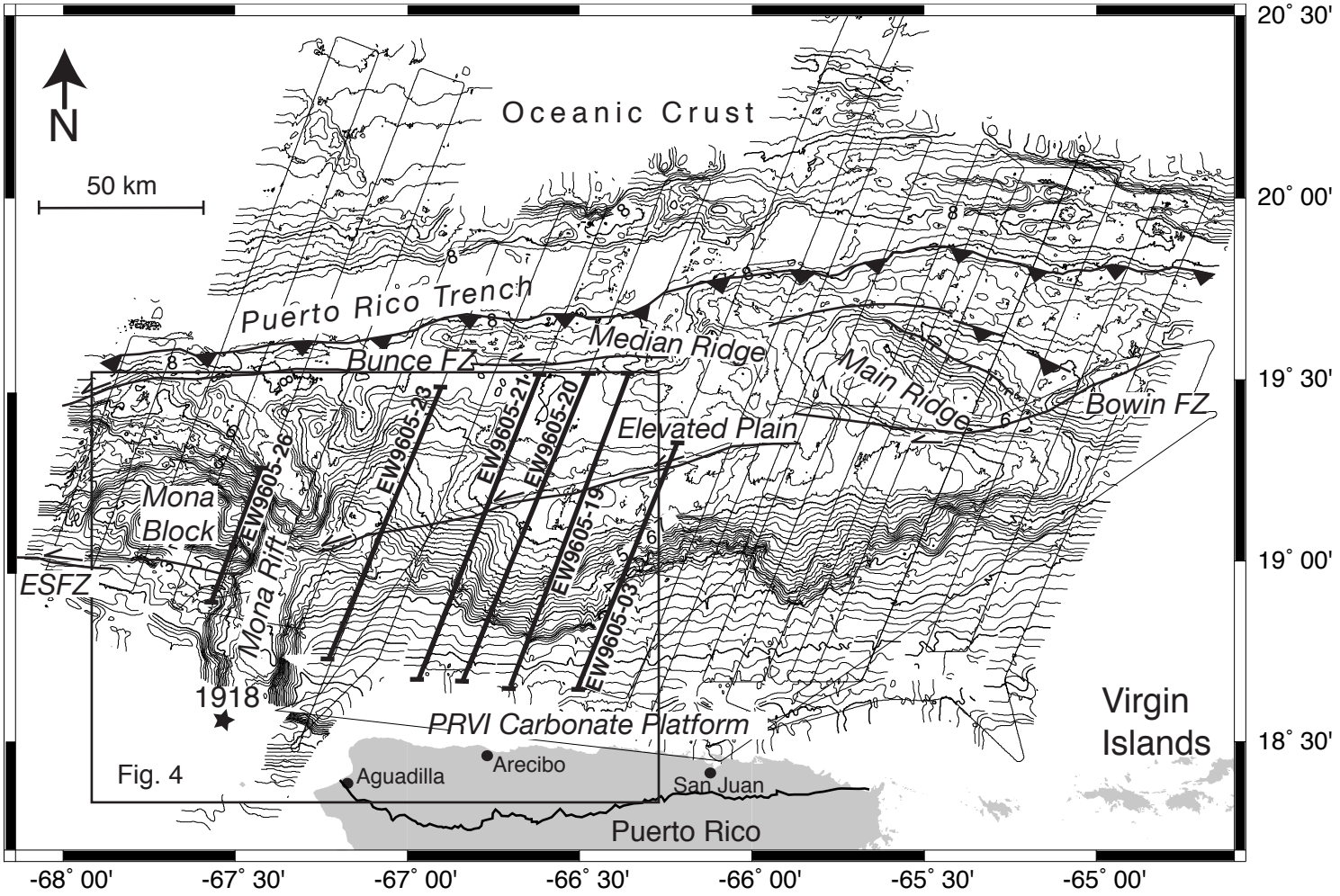
N
50 km
Oceanic Crust
Puerto Rico Trench
Bunce FZ
Median Ridge
Main Ridge
Bowin FZ
Elevated Plain
Mona Block
Mona Rift
ESFZ
EW9605-26
EW9605-23
EW9605-21
EW9605-20
EW9605-19
EW9605-03
1918
PRVI Carbonate Platform
Fig. 4
Aguadilla
Arecibo
San Juan
Puerto Rico
Virgin Islands
20˚ 30'
20˚ 00'
19˚ 30'
19˚ 00'
18˚ 30'
-68˚ 00'
-67˚ 30'
-67˚ 00'
-66˚ 30'
-66˚ 00'
-65˚ 30'
-65˚ 00'

Figure 4. a) EW96-05 Hydrosweep bathymetry data of the study area; grid cell size is 250 m; contours are at 200 m. White arrows indicate the presumed direction of sediment and submarine landslide debris transport toward final deposition on the main trench axis. Circles show location of the core data documenting a giant sand turbidite and overlying lutite turbidites. See table 1 for core descriptions. Erosional gullies are labeled by blue springs along the headscarp margin. The location of the onshore CPR-4 well and major north coast cities relative to the scarp is shown.

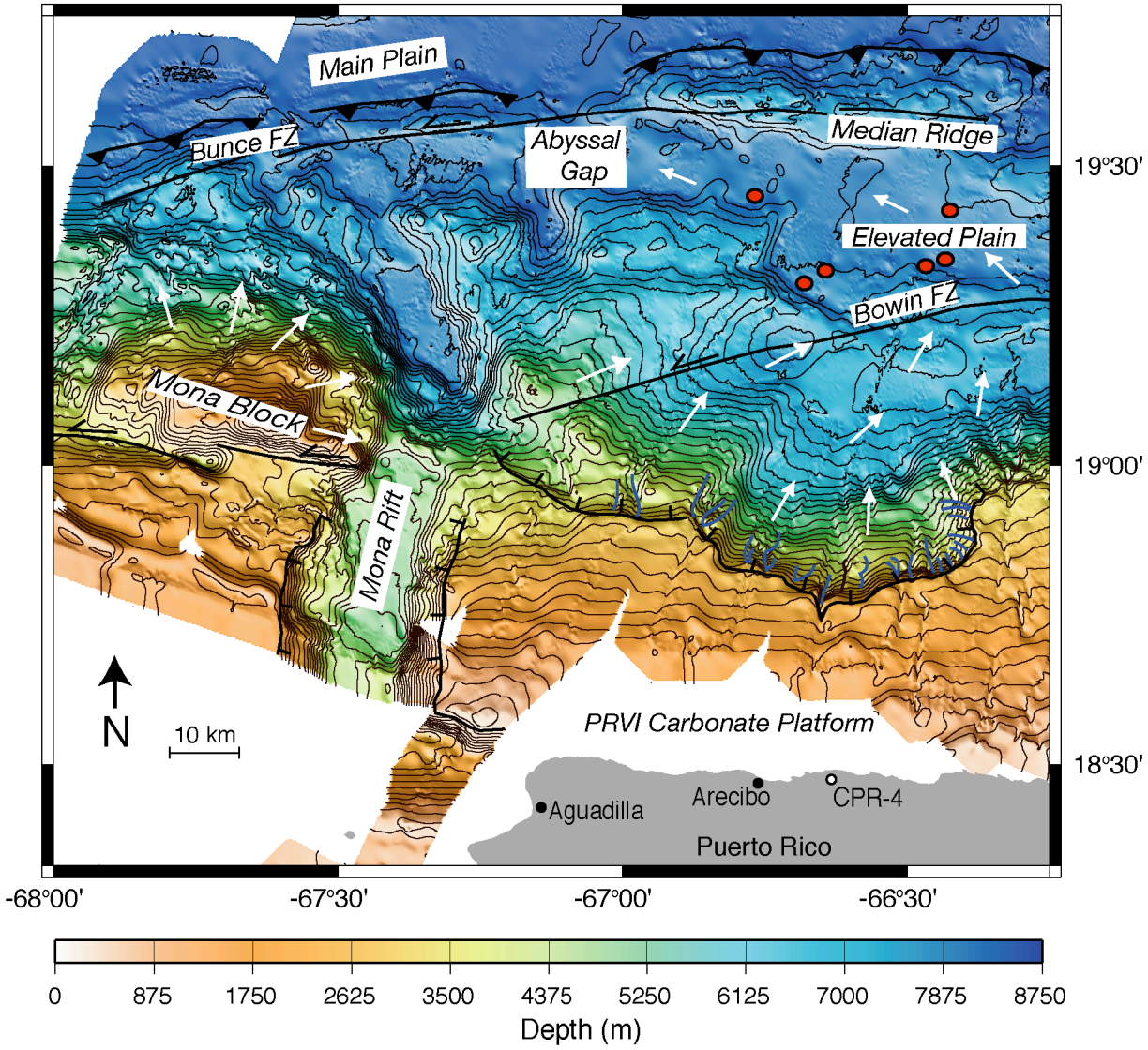
Main Plain
Bunce FZ
Abyssal Gap
Median Ridge
Elevated Plain
Bowin FZ
Mona Block
Mona Rift
N
10 km
PRVI Carbonate Platform
Aguadilla
Arecibo
CPR-4
Puerto Rico
19°30'
19°00'
18°30'
-68°00'
-67°30'
-67°00'
-66°30'
0
875
1750
2625
3500
4375
5250
6125
7000
7875
8750
Depth (m)

Figure 4. b) HMR1 sidescan imagery of the amphitheater-shaped scarp, including the Mona Block and the Median Ridge. ESFZ = the East Septentroinal Fault Zone. Grid interval = 17 m. Areas of high backscatter (dark color) are interpreted as coarse-grained, unorganized landslide debris on the seafloor or reef material. Low backscatter (light color) regions reflect the presence of fine-grained sands, pelagic sediment, or slumped PRVI carbonate platform. White areas are data gaps. Boxes show the location of sidescan sonar images in figures 7and 10. The location of the onshore CPR-4 well and major north coast cities relative to the scarp is shown

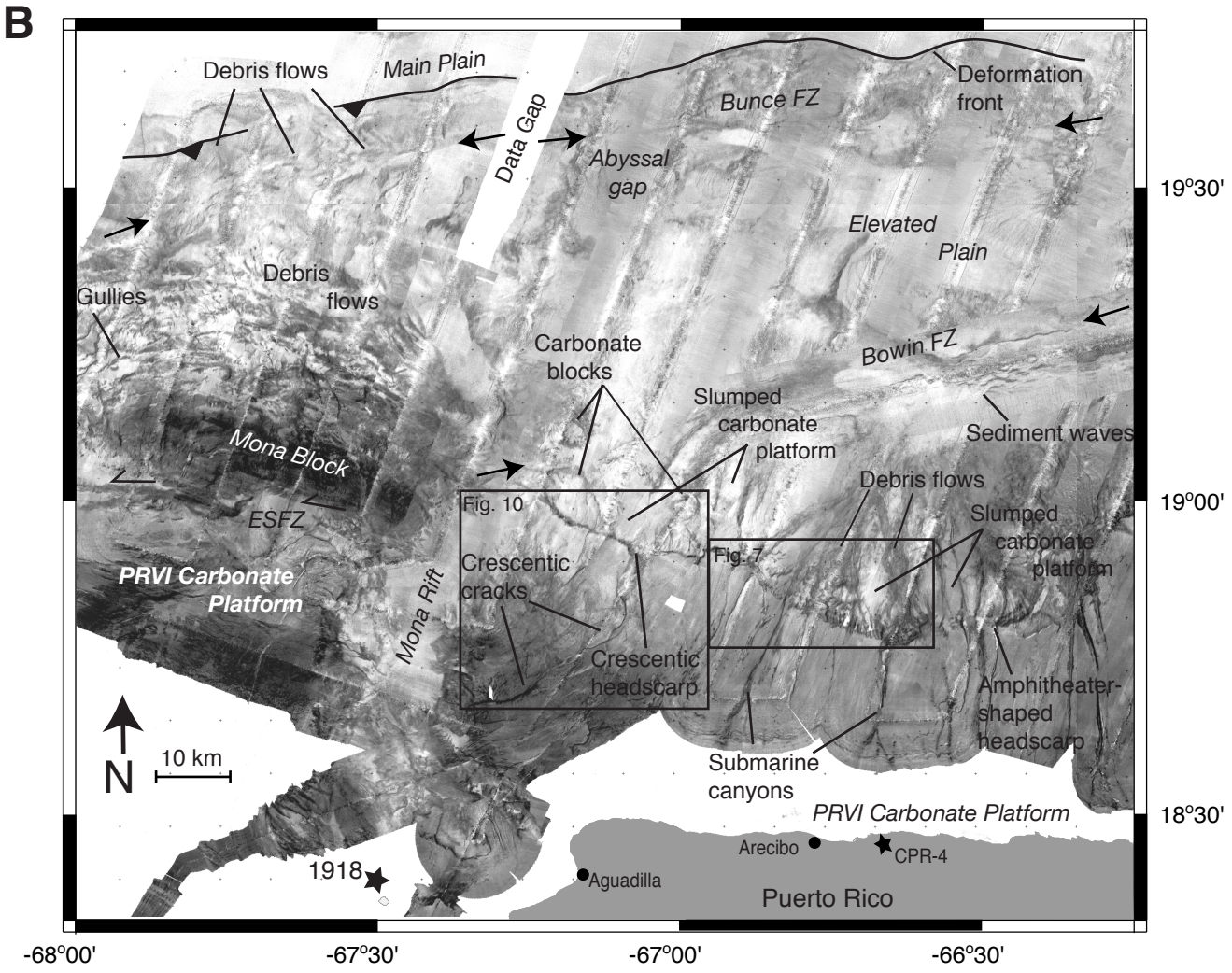
B
Debris flows
Main Plain
Data Gap
Abyssal gap
Bunce FZ
Deformation front
Elevated Plain
Gullies
Debris flows
Carbonate blocks
Bowin FZ
Slumped carbonate platform
Sediment waves
Mona Block
ESFZ
Fig. 10
Fig. 7
Debris flows
Slumped carbonate platform
PRVI Carbonate Platform
Mona Rift
Crescentic cracks
Crescentic headscarp
Amphitheater-shaped headscarp
Submarine canyons
N
10 km
PRVI Carbonate Platform
Arecibo
CPR-4
1918
Aguadilla
Puerto Rico
19°30'
19°00'
18°30'
-68°00'
-67°30'
-67°00'
-66°30'

Figure 4. c) Sidescan sonar of area draped over the Hydrosweep bathymetry grid looking from NE to SW. The locations of the single-channel seismic profile lines are shown as dashed black lines. V.E. is 6:1.

C

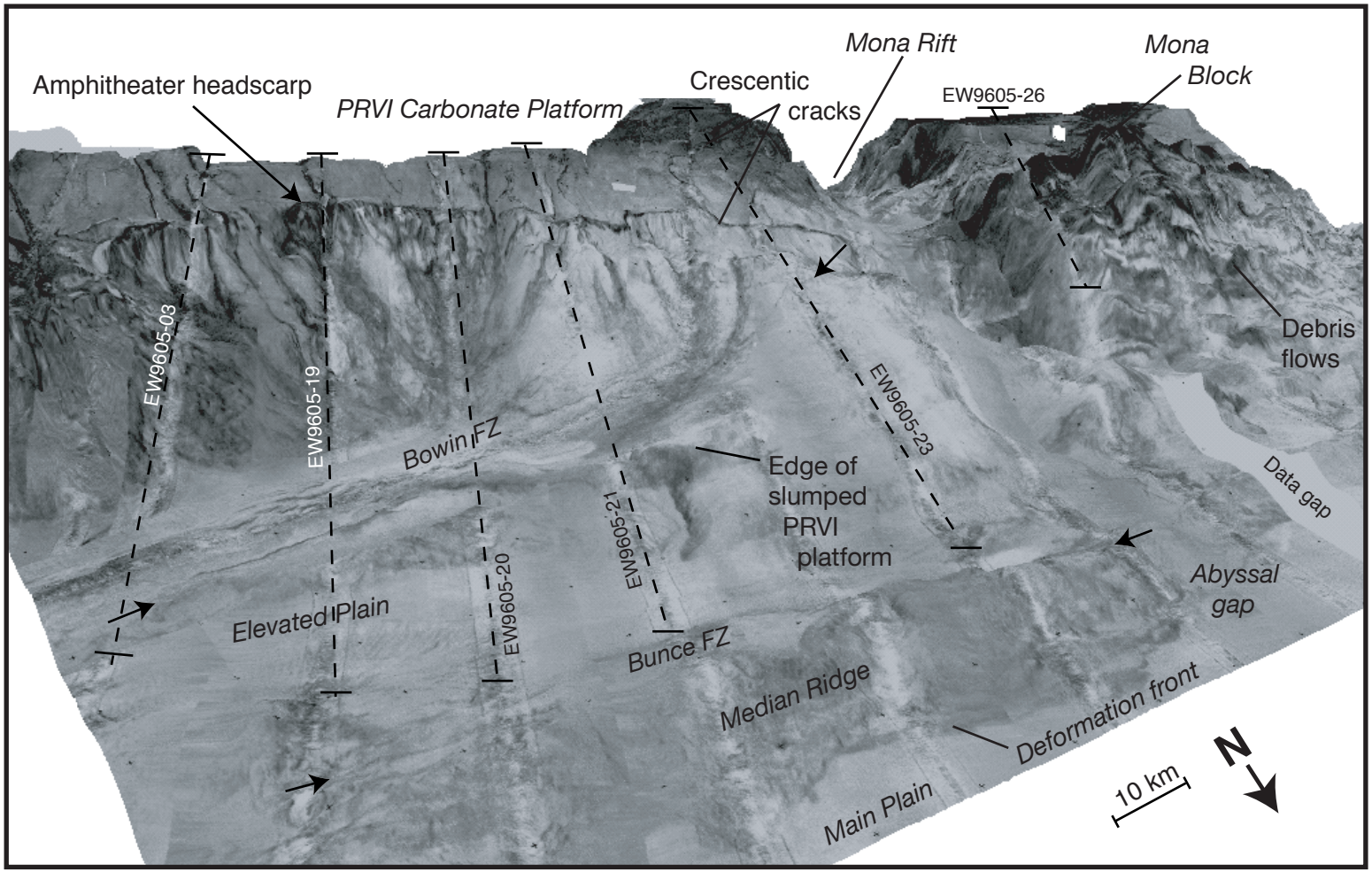
Amphitheater headscarp
PRVI Carbonate Platform
Crescentic cracks
Mona Rift
Mona Block
EW9605-26
Debris flows
EW9605-03
EW9605-19
Bowin FZ
EW9605-20
EW9605-21
Edge of slumped PRVI platform
EW9605-23
Data gap
Abyssal gap
Elevated Plain
Bunce FZ
Median Ridge
Deformation front
Main Plain
10 km
N

Figure 5. Interpreted line drawings of part of EW9605 seismic lines 21, 20, 19, and 3 extending seaward of the amphitheater-shaped scarp. Sub-seafloor reflectors show that submarine landslide deposits north of the amphitheater are predominately extensive, stacked turbidite deposits. Inset shows the location of the line relative to the north coast of Puerto Rico and the seaward edge of the PRVI platform. V.E. is approximately ~ 4.0.

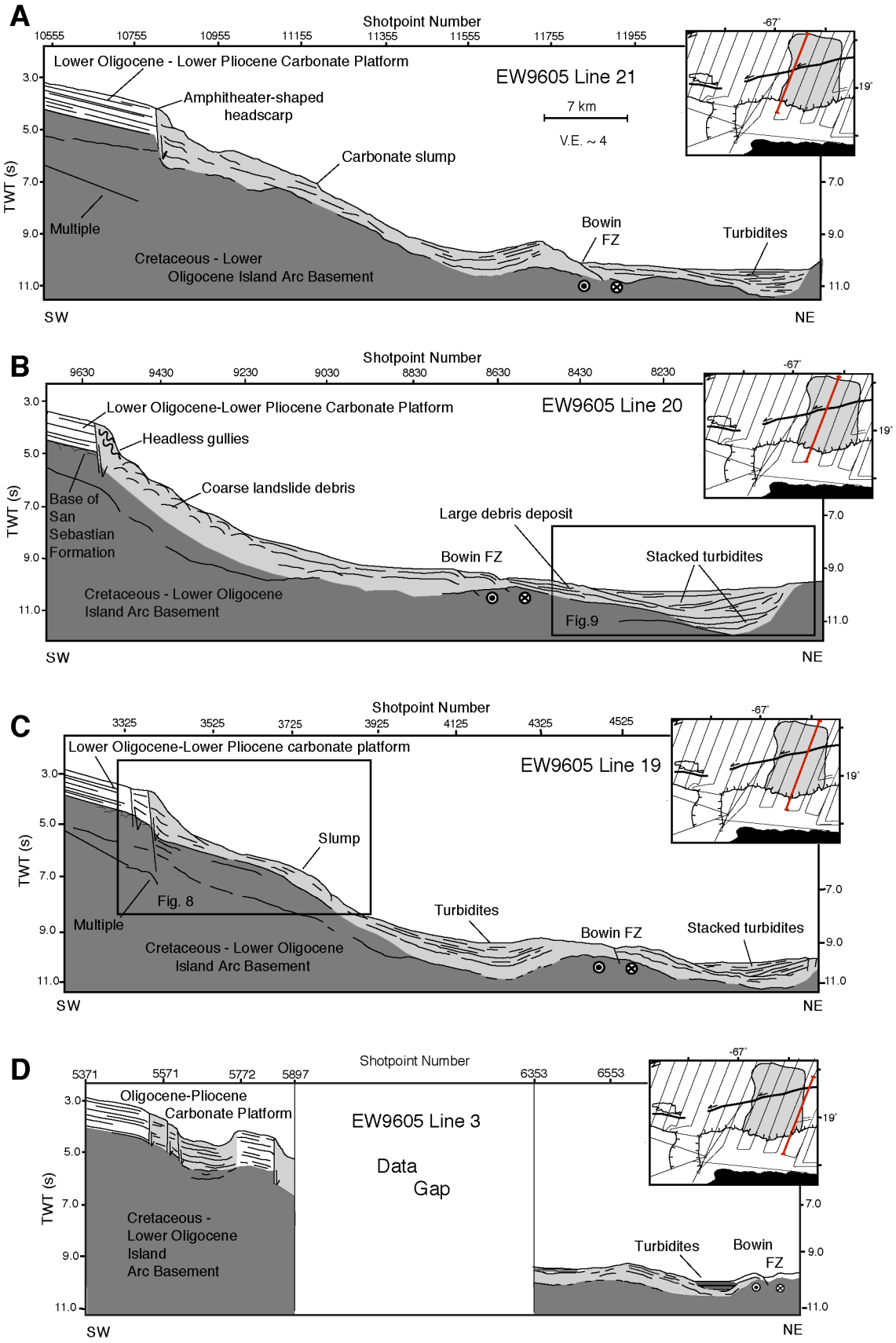
A
Shotpoint Number
10555
10755
10955
11155
11355
11555
11755
11955
Lower Oligocene - Lower Pliocene Carbonate Platform
EW9605 Line 21
7 km
V.E. ~ 4
Amphitheater-shaped headscarp
Carbonate slump
Multiple
Cretaceous - Lower Oligocene Island Arc Basement
Bowin FZ
Turbidites
TWT (s)
SW
NE
B
Shotpoint Number
9630
9430
9230
9030
8830
8630
8430
8230
Lower Oligocene-Lower Pliocene Carbonate Platform
EW9605 Line 20
Headless gullies
Coarse landslide debris
Base of San Sebastian Formation
Large debris deposit
Bowin FZ
Stacked turbidites
Cretaceous - Lower Oligocene Island Arc Basement
Fig.9
C
Shotpoint Number
3325
3525
3725
3925
4125
4325
4525
Lower Oligocene-Lower Pliocene carbonate platform
EW9605 Line 19
Slump
Fig. 8
Multiple
Turbidites
Bowin FZ
Stacked turbidites
Cretaceous - Lower Oligocene Island Arc Basement
D
Shotpoint Number
5371
5571
5772
5897
6353
6553
Oligocene-Pliocene Carbonate Platform
EW9605 Line 3
Data Gap
Cretaceous - Lower Oligocene Island Arc Basement
Turbidites
Bowin FZ
-67°
19°
3.0
5.0
7.0
9.0
11.0

Figure 6. Geological interpretation of the study area based on bathymetry, sidescan sonar, SCS, and core data. Structural features include the Bowin, Bunce, and Septentroinal fault zones, the main headscarp, the crescentic-shaped headwall to the west, crescentic cracks along the eastern flank of the Mona Rift, the Mona Block, and the Median Ridge. The extent of intact carbonate strata and submarine landslide deposits is shown. Location of core data is represented by open circles. The northern margin of the PRVI carbonate platform is cut by submarine canyons and eroded by headless gullies (gray squiggles).

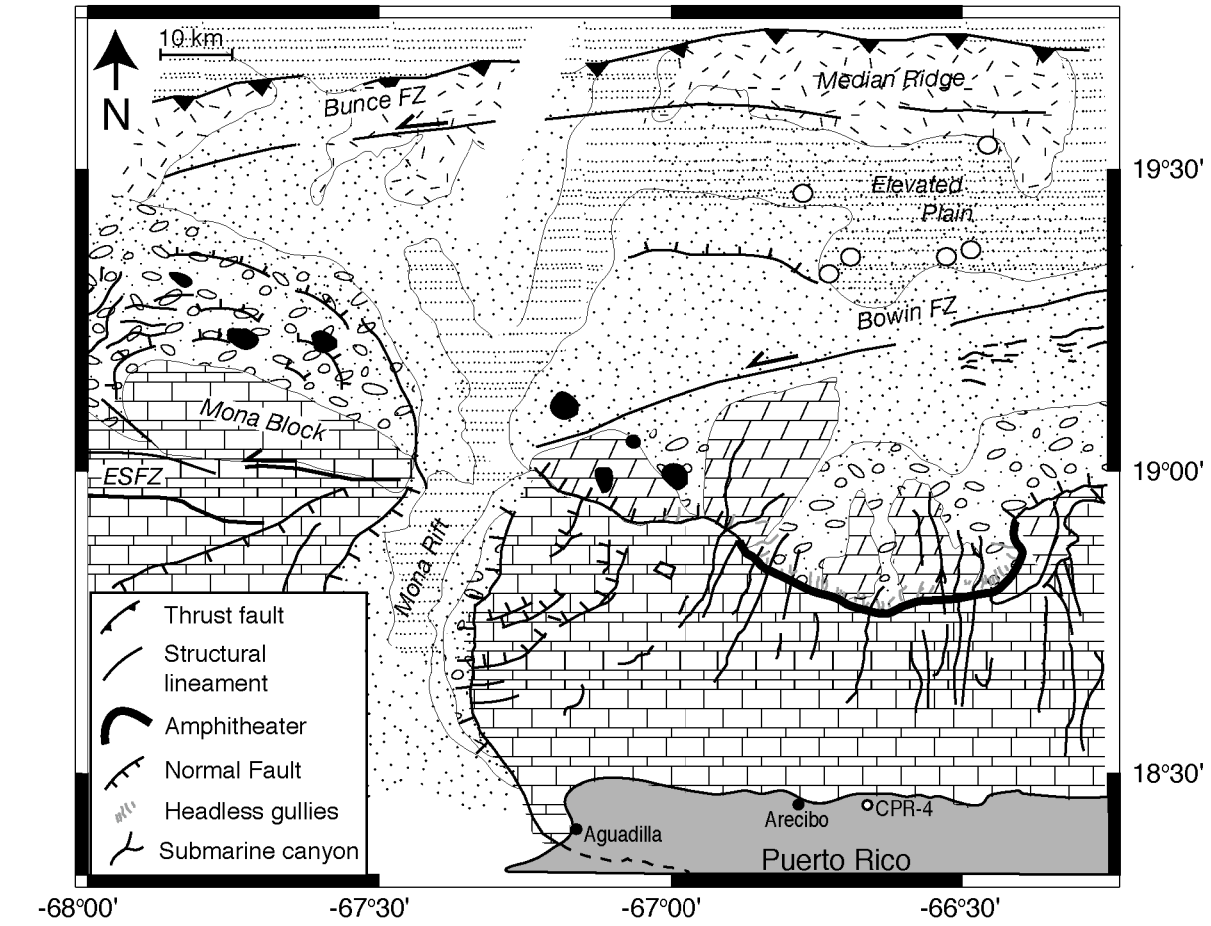
10 km
N
Bunce FZ
Median Ridge
Elevated Plain
Bowin FZ
Mona Block
ESFZ
Mona Rift
Thrust fault
Structural lineament
Amphitheater
Normal Fault
Headless gullies
Submarine canyon
Aguadilla
Arecibo
CPR-4
Puerto Rico
19°30'
19°00'
18°30'
-68°00'
-67°30'
-67°00'
-66°30'
PRVI Carbonate Platform
Well-bedded turbidites
Slumped carbonate
Blocks
Debris flow
Turbidites
Forearc with pelagic drape

Figure 7. HMR1 sidescan sonar imagery along the amphitheater margin and adjacent crescentic-shaped headscarp. Areas of high backscatter (dark color) are interpreted as coarse-grained, shelf material or blocky, submarine landslide deposits. The areas of low backscatter (light color) reflect the presence of fine-grained sands, slump portions of the carbonate platform, and the intact, upper-slope forming PRVI carbonate platform south of the headscarp margin. Grid interval = 17 m. a westward decrease in gullying along the northern margin of the carbonate platform is observed within the study area.

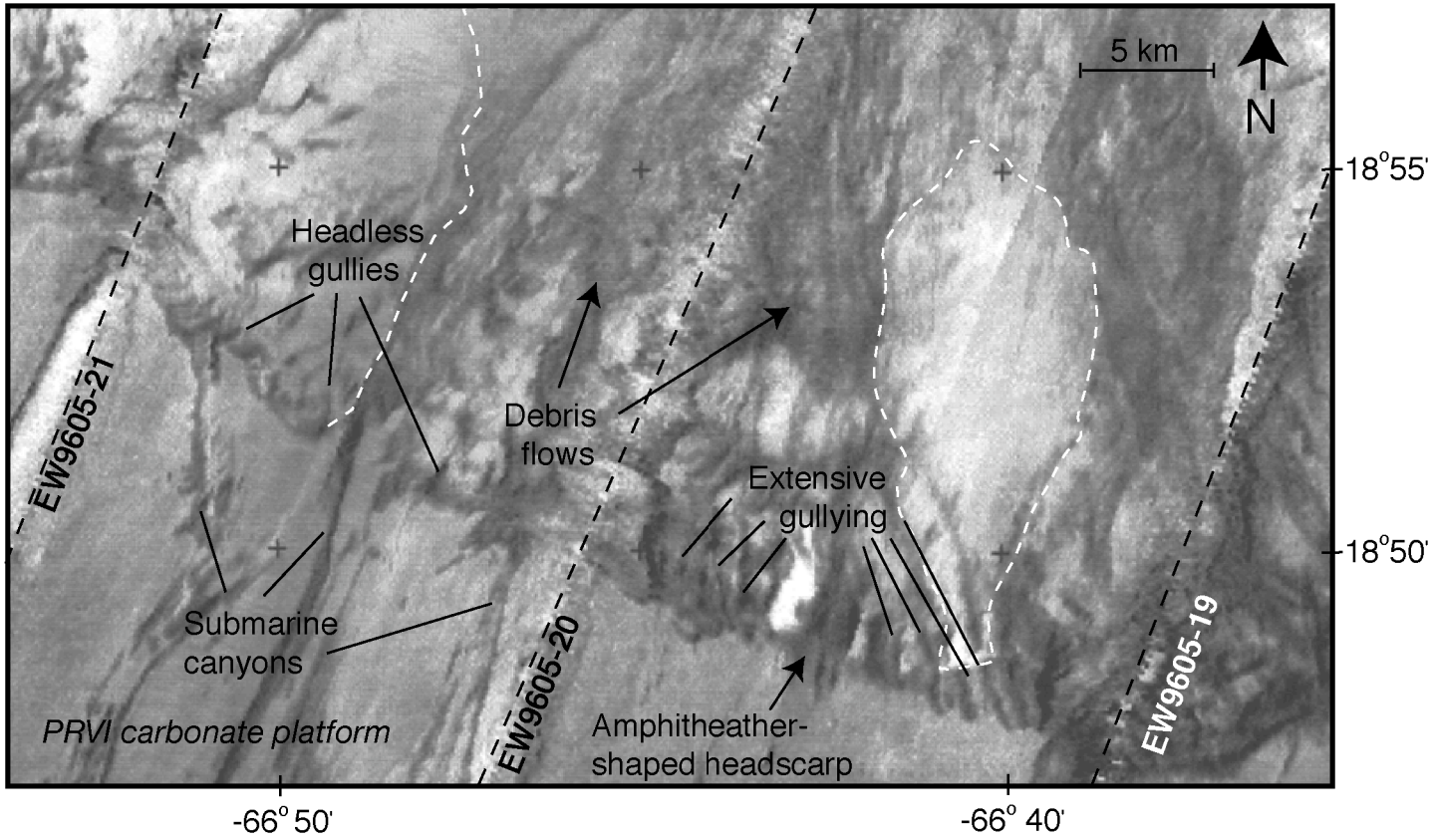
5 km
N
18°55'
18°50'
-66° 50'
-66° 40'
Headless gullies
Debris flows
Extensive gullying
Submarine canyons
PRVI carbonate platform
Amphitheather-shaped headscarp
EW9605-21
EW9605-20
EW9605-19

Figure 8. a) Part of EW9605 SCS line 19 shows offset in the headscarp extends into underlying island arc basement material (location given in figure 5). MCS data collected by Meyerhoff et al. (1980) show scarp fault penetrating the volcaniclastic basement rock. A slumped package of PRVI carbonate strata is imaged on the face of the scarp along a resolvable glide plane. b) Interpreted line drawing of a.

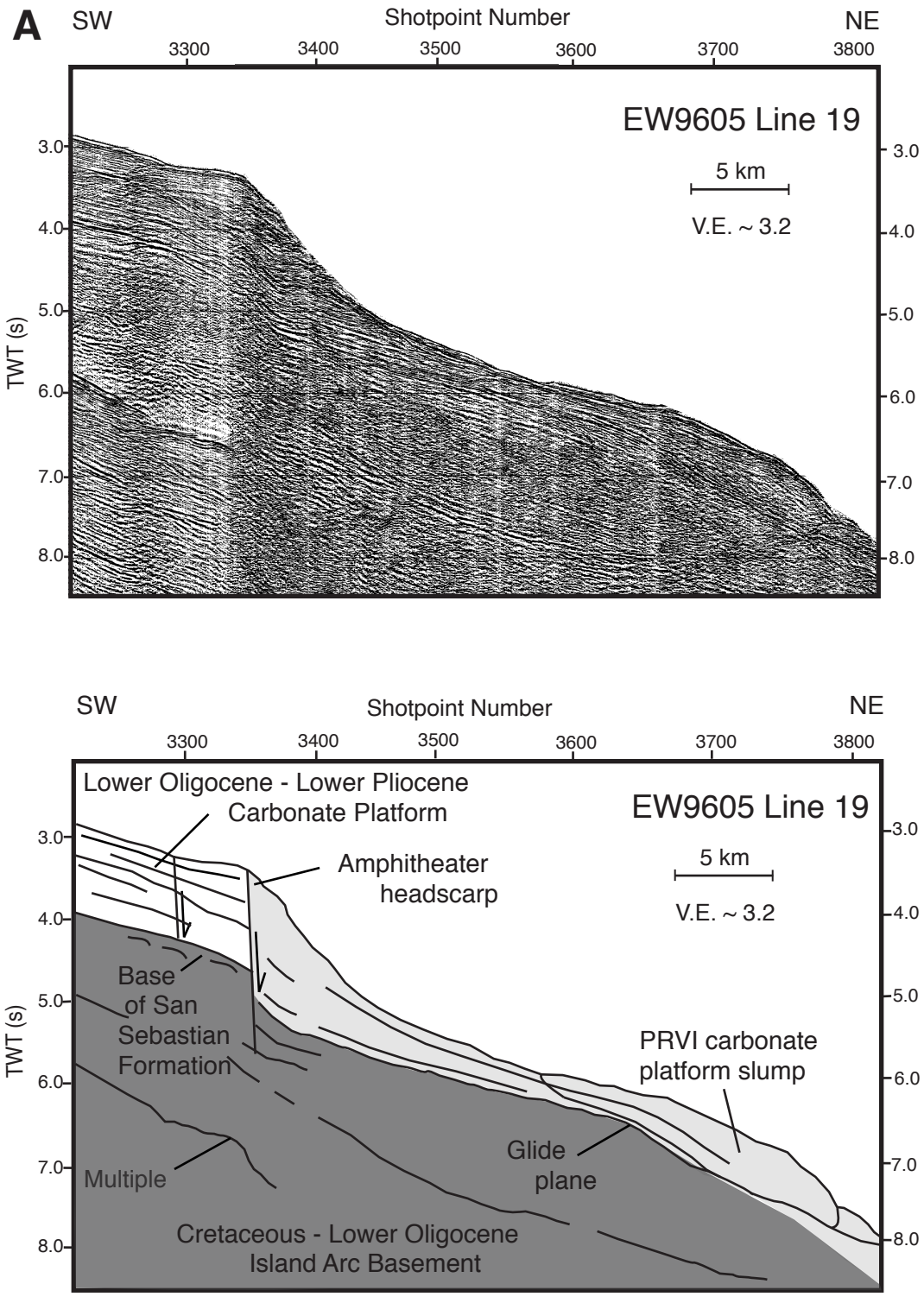
A
SW
Shotpoint Number
NE
3300
3400
3500
3600
3700
3800
EW9605 Line 19
5 km
V.E. ~ 3.2
TWT (s)
3.0
4.0
5.0
6.0
7.0
8.0
SW
Shotpoint Number
NE
Lower Oligocene - Lower Pliocene
Carbonate Platform
Amphitheater
headscarp
Base
of San
Sebastian
Formation
PRVI carbonate
platform slump
Glide
plane
Multiple
Cretaceous - Lower Oligocene
Island Arc Basement

Figure 9. a) Part of EW9605 SCS line 20 seaward of the amphitheater-shaped scarp. North of the Bowin Fault on the Elevated Plain at least 8 packages of sediment, constituting an infilling of up to 1.6 km in thickness (@ 1.8 m/s), are back-tilted along the southern flank of the Median Ridge. The larger of these deposits can be traced from the base-of-slope to its deposition on the Elevated Plain, 60 km north of the headscarp crown. b) Interpreted line drawing of a.

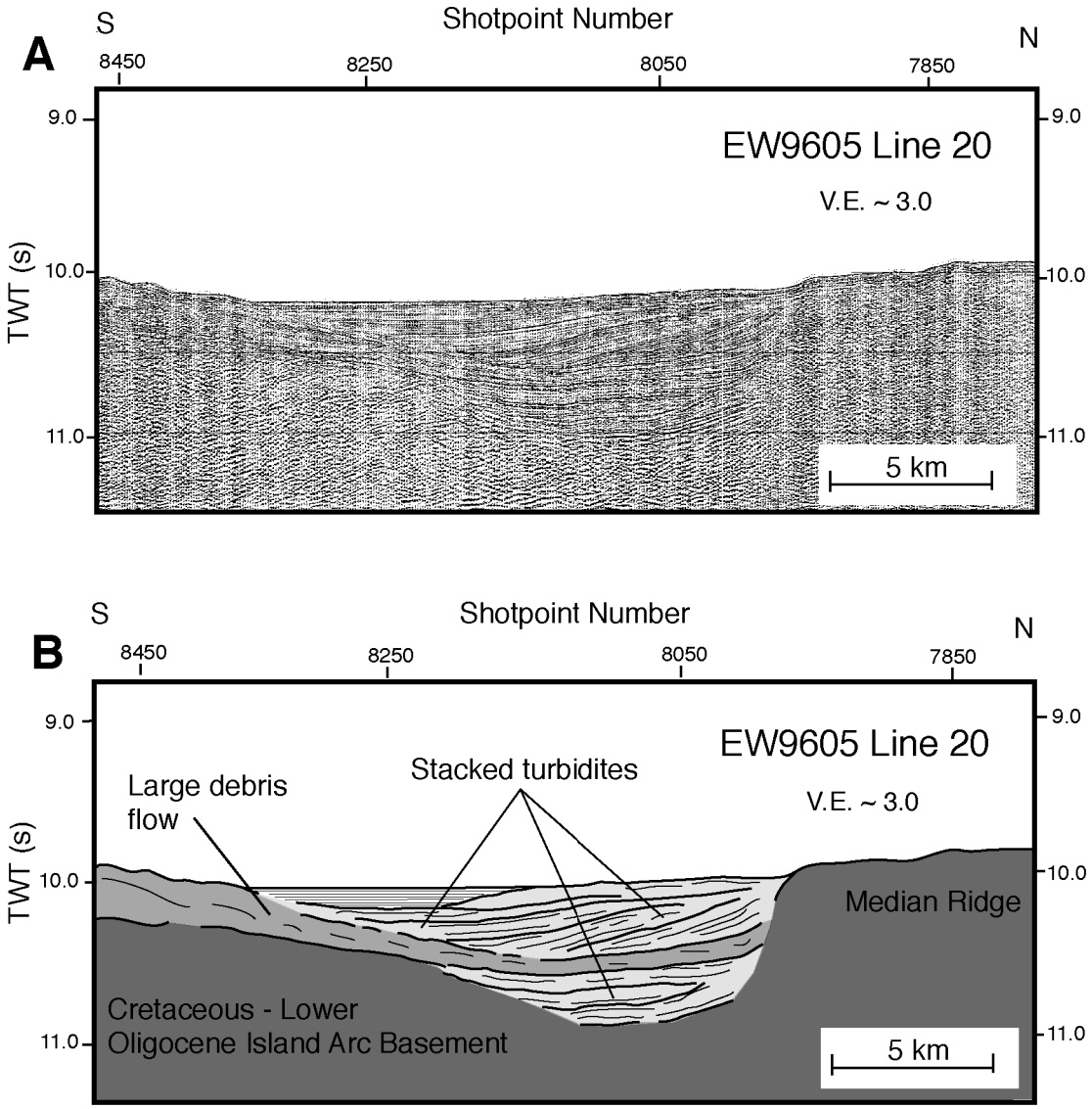
A
S
Shotpoint Number
N
8450
8250
8050
7850
9.0
10.0
11.0
TWT (s)
EW9605 Line 20
V.E. ~ 3.0
5 km
B
S
Shotpoint Number
N
8450
8250
8050
7850
9.0
10.0
11.0
TWT (s)
EW9605 Line 20
V.E. ~ 3.0
Large debris flow
Stacked turbidites
Median Ridge
Cretaceous - Lower Oligocene Island Arc Basement
5 km

Figure 10. HMR1 sidescan sonar imagery of the *en echelon*, crescentic cracks and the southwestern margin of the crescentic-shaped headscarp offshore the WNW coast of Puerto Rico. Areas of highly reflective seafloor are shown as dark returns, seafloor with low reflectivity is light. Grid interval = 17 m.

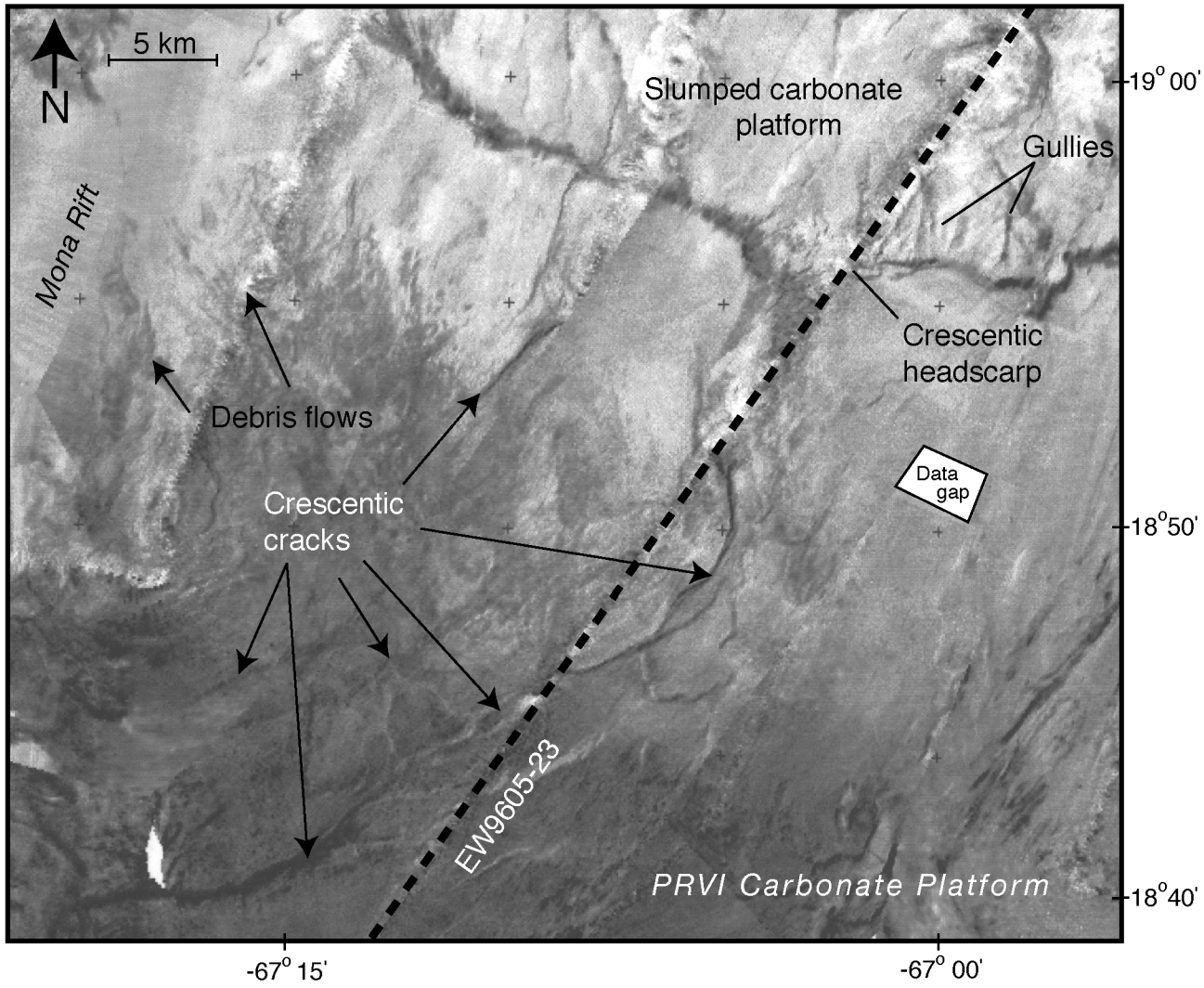
5 km
N
Slumped carbonate platform
Gullies
Mona Rift
Crescentic headscarp
Debris flows
Data gap
Crescentic cracks
EW9605-23
PRVI Carbonate Platform
19° 00'
18°50'
18°40'
-67° 15'
-67° 00'

Figure 11. Interpreted line drawing of EW9605 SCS line 23 extending trenchward of the E-SE trending crescentic-shaped headscarp. Note the abundant fracturing of the northwestern margin of the PRVI platform. Inset shows the location of the SCS line relative to the north coast of Puerto Rico and the seaward edge of the PRVI platform. Boxed area shows location of Figures 12 and 13.

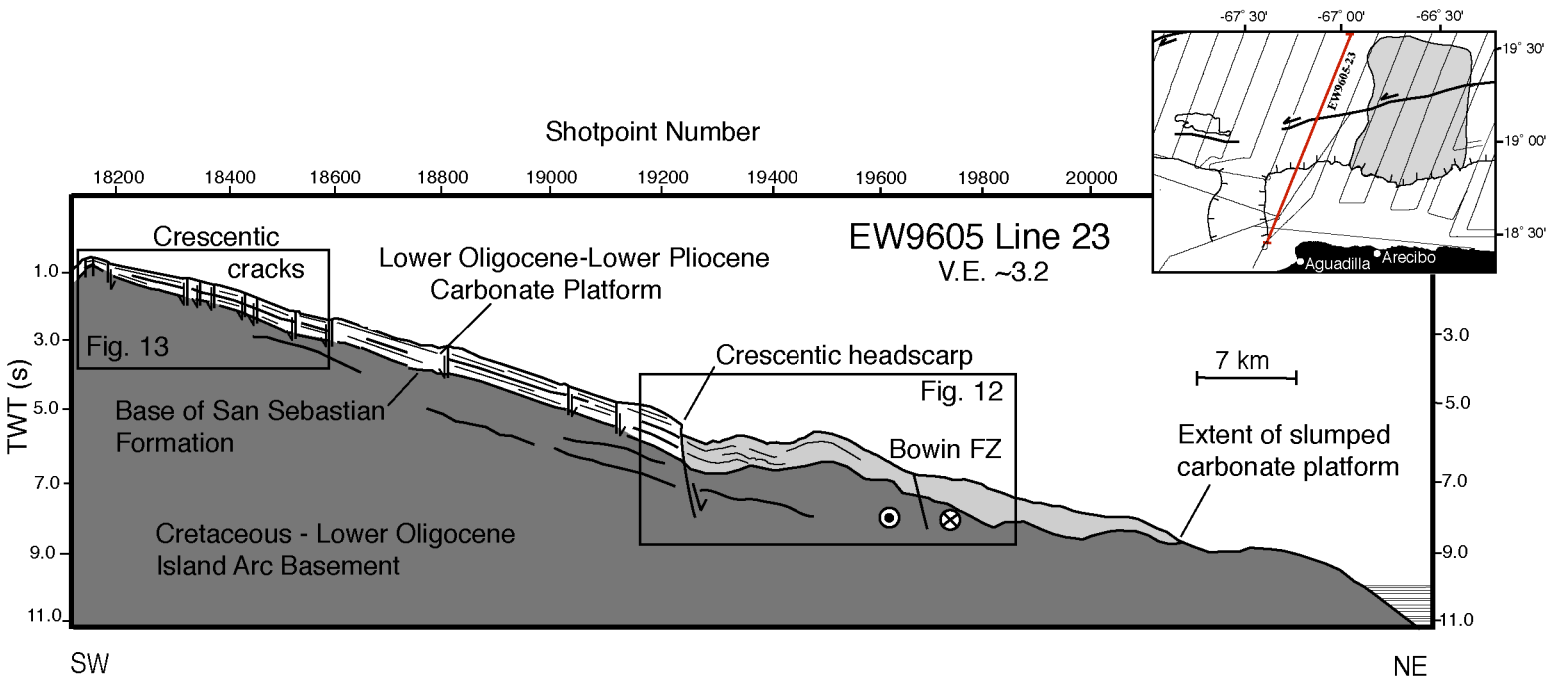
Shotpoint Number
18200
18400
18600
18800
19000
19200
19400
19600
19800
20000
EW9605 Line 23
V.E. ~3.2
Crescentic
cracks
Fig. 13
Lower Oligocene-Lower Pliocene
Carbonate Platform
Crescentic headscarp
Fig. 12
Bowin FZ
Base of San Sebastian
Formation
Cretaceous - Lower Oligocene
Island Arc Basement
Extent of slumped
carbonate platform
7 km
TWT (s)
1.0
3.0
5.0
7.0
9.0
11.0
SW
NE
-67° 30'
-67° 00'
-66° 30'
19° 30'
19° 00'
18° 30'
EW9605-23
Aguadilla
Arecibo

Figure 12. a) Part of EW9605 SCS line 23 showing the crescentic-shaped headscarp and 750-m thick down-dropped portion of PRVI carbonate material. The PRVI carbonate platform has begun to collapse trenchward over an area of roughly 500 km^2 equivalent to a volume of 375 km^3. b) Interpreted line drawing of SCS profile.

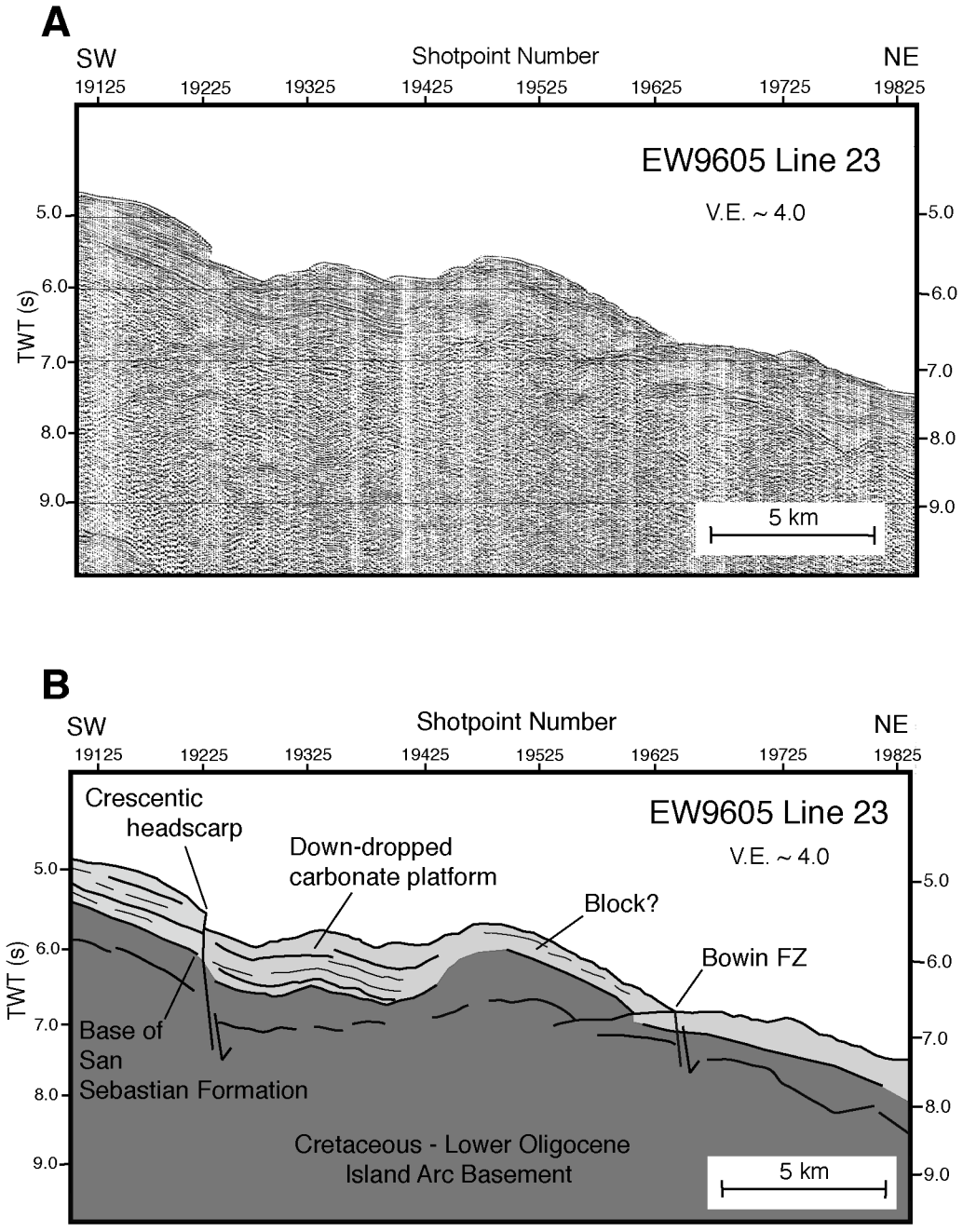
A
SW
Shotpoint Number
NE
19125
19225
19325
19425
19525
19625
19725
19825
EW9605 Line 23
V.E. ~ 4.0
TWT (s)
5.0
6.0
7.0
8.0
9.0
5 km
B
SW
Shotpoint Number
NE
Crescentic headscarp
Down-dropped carbonate platform
Block?
Bowin FZ
EW9605 Line 23
V.E. ~ 4.0
Base of San Sebastian Formation
Cretaceous - Lower Oligocene Island Arc Basement
5 km

Figure 13. a) Part of EW9605 SCS line 23 shows the extensive fracturing of the PRVI carbonate platform along the eastern flank of the Mona Rift. b) Interpreted line drawing of a. Figure 10 shows the sidescan sonar record of these seafloor features.

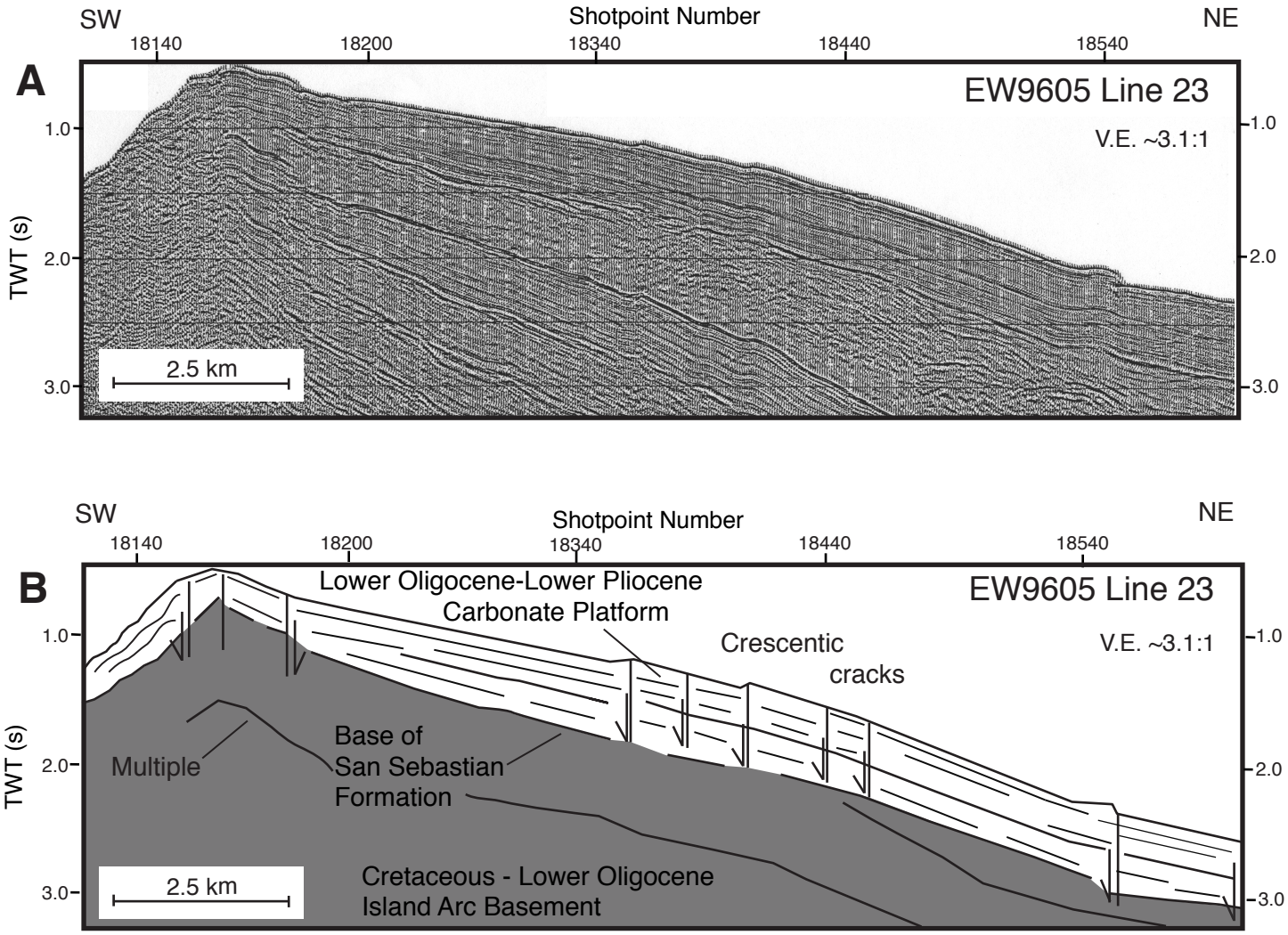
A
SW
Shotpoint Number
NE
18140
18200
18340
18440
18540
EW9605 Line 23
V.E. ~3.1:1
TWT (s)
1.0
2.0
3.0
2.5 km
B
Lower Oligocene-Lower Pliocene
Carbonate Platform
Crescentic
cracks
Multiple
Base of
San Sebastian
Formation
Cretaceous - Lower Oligocene
Island Arc Basement

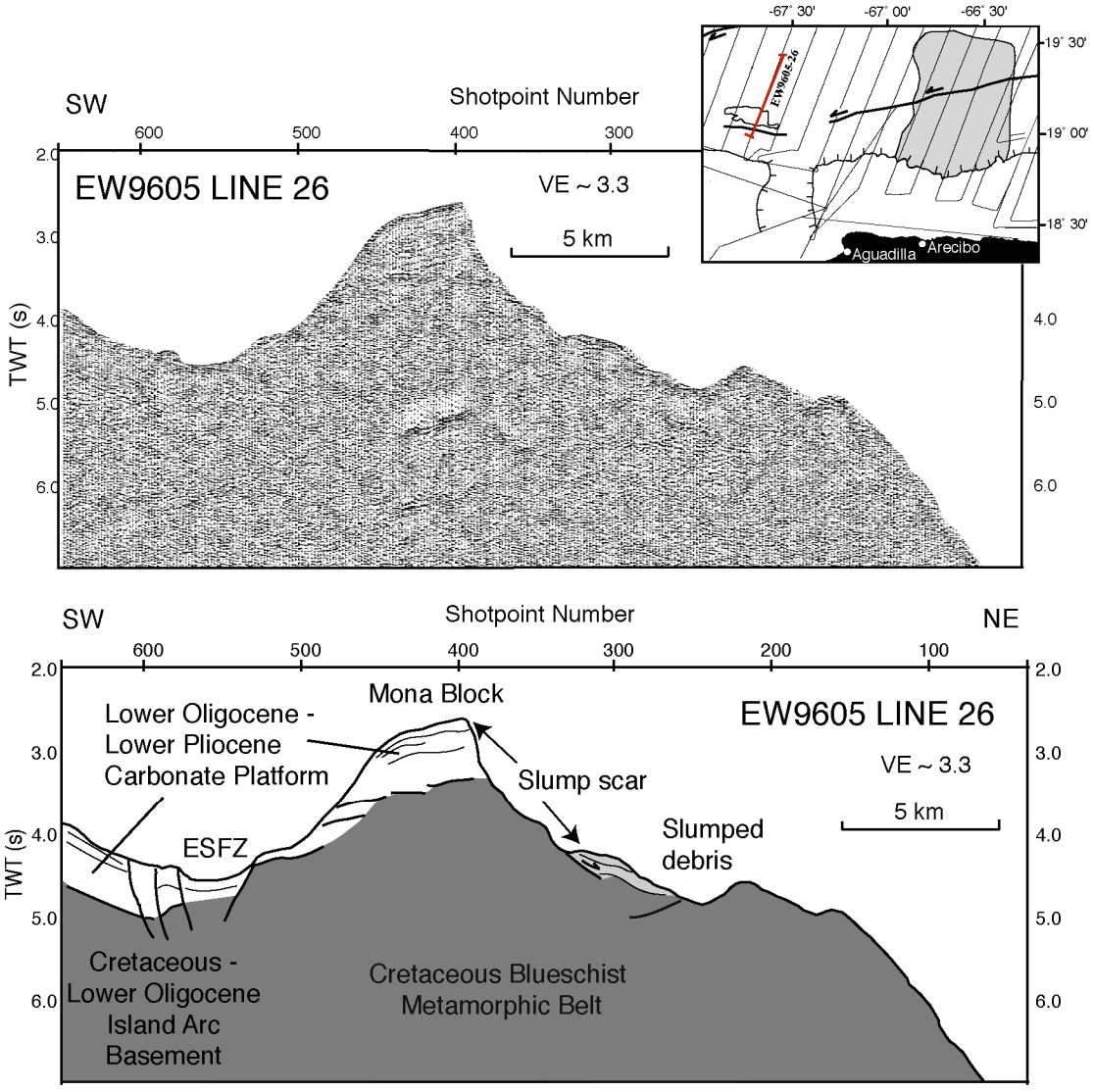

Figure 14. Part of EW9605 SCS line 26 across the northwest carbonate platform, the East Septentroinal Fault Zone (ESFZ), and Mona Block. The parallel reflector in the upper section of the Mona Block is interpreted as part of the carbonate platform uplifted by the underthrusting of the SE Bahamas Province (Grindlay et al., 2004). Inset shows location of the SCS line relative to the north coast of Puerto Rico and the seaward edge of the PRVI platform.

Figure 15. Series of grids used to calculate the area and volume of the Puerto Rico submarine landslide. Inset a is the simplified reconstructed slope surface of the northern PRVI margin prior to the landslide (Surface 1). Surface 1 was created by replacing the landslide void with interpolated bathymetric contours across the eastern and western walls of the scarp. Inset b is a grid of the present-day seafloor topography (Surface 2). Inset c is a cartoon of the bathymetry profiles over the intact and failed sections of the PRVI margin showing cross sections of Surfaces 1-3. Surface 3 is the base of the landslide deposit. V1 = Surface 2 – Surface 1 (volume of upper-voided slope); V2 = Surface 3 – Surface 2 (volume of entire submarine landslide debris field). Inset d is a map of the landslide thickness in meters below sea level (Surface 3 – Surface 2). The seismic profile data were used to pick the base-of-landslide horizon and time was converted to depth using a two-way travel time of 1.8 km/s. Inset e is the submarine landslide deposit isopach map (Surface 3 – Surface 2).

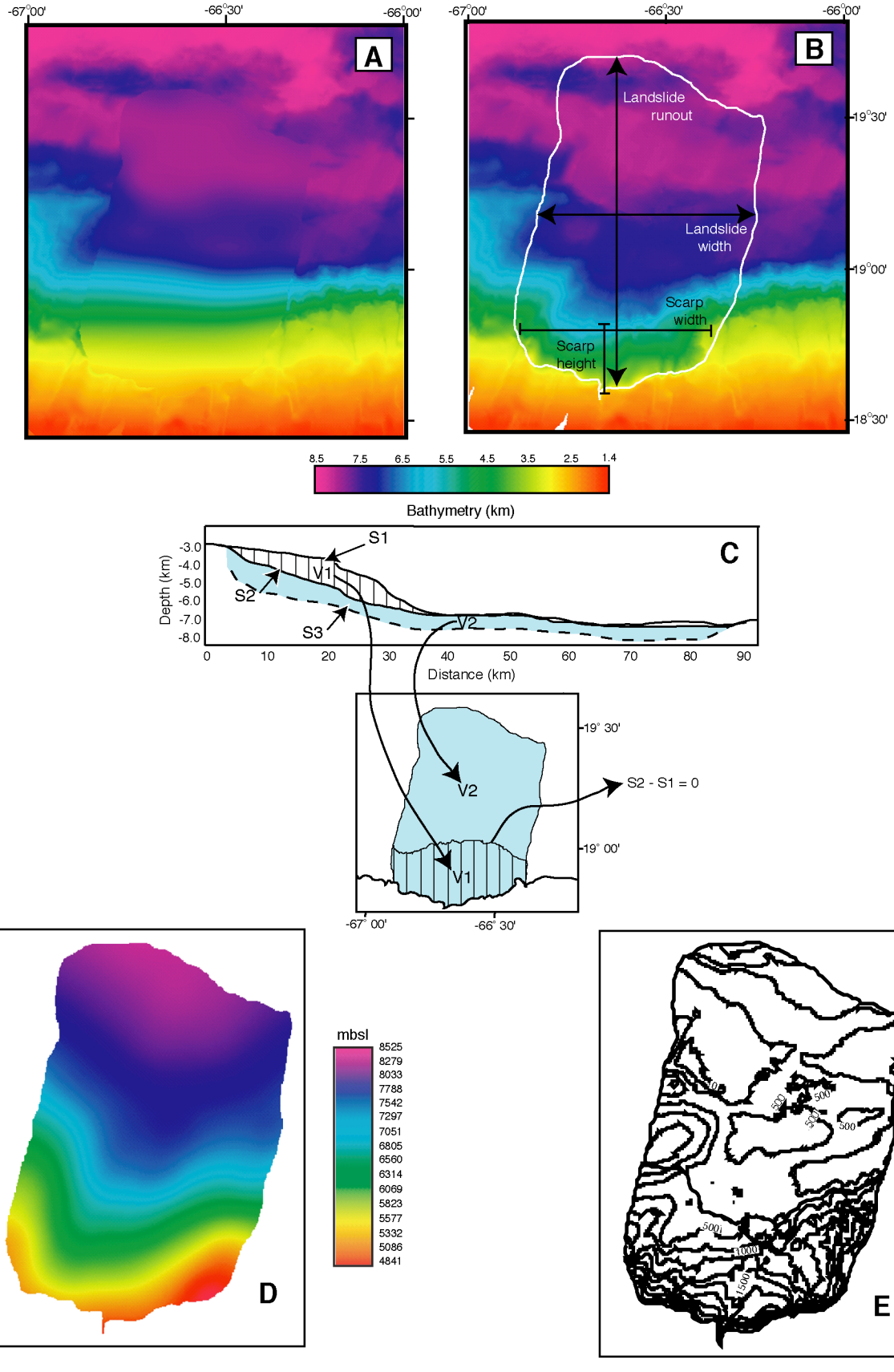
-67°00'
-66°30'
-66°00'
A
B
Landslide runout
Landslide width
Scarp width
Scarp height
19°30'
19°00'
18°30'
8.5 7.5 6.5 5.5 4.5 3.5 2.5 1.4
Bathymetry (km)
C
S1
S2
S3
V1
V2
Depth (km)
-3.0
-4.0
-5.0
-6.0
-7.0
-8.0
0 10 20 30 40 50 60 70 80 90
Distance (km)
19° 30'
19° 00'
S2 - S1 = 0
-67° 00'
-66° 30'
mbsl
8525
8279
8033
7788
7542
7297
7051
6805
6560
6314
6069
5823
5577
5332
5086
4841
D
500
1000
1500
E

Figure 16. a) 2-D shaded relief bathymetry of the Mona Block region showing major seafloor features inferred to be associated with the subduction of the SE Bahamas Province. b) Schematic taken from Dominguez et al. (1998) showing the typical fault network generated by the subduction of a seamount. A similar diverging fault networking is seen along the northwestern PRVI margin where Grindlay et al. (2004) propose the SE Bahamas Province is being subducted beneath the Caribbean plate (Inset a). c) Schematic showing the time-transgressive location of the SE extension of the Bahamas Province relative to the amphitheater and crescentic-shaped headscarp and cracks along the northern PRVI margin. The dashed black lines indicate the position of the overthickened (20+ km) oceanic crust associated with the SE Bahamas, assuming present-day relative plate motion. The subducted high is currently colliding with the northwestern PRVI margin, possibly prompting submarine landslides at this location, presumably along the crescentic-shaped headscarp.

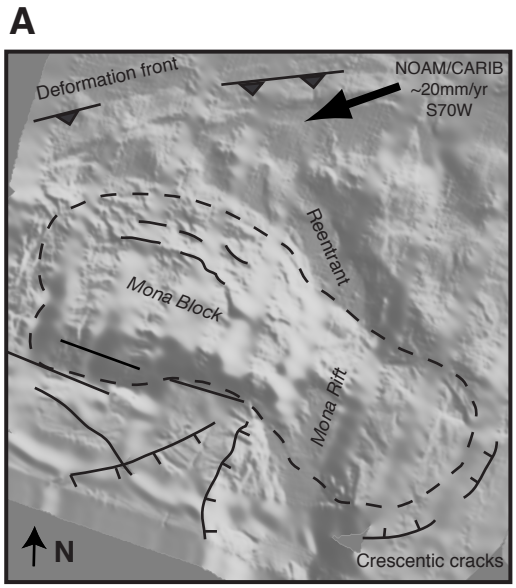
A
Deformation front
NOAM/CARIB
~20mm/yr
S70W
Reentrant
Mona Block
Mona Rift
N
Crescentic cracks

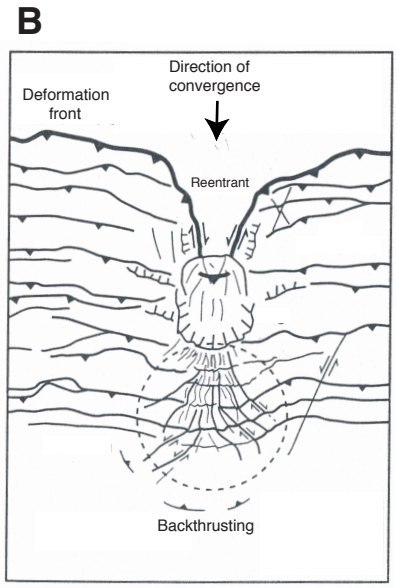
B
Direction of
convergence
Deformation
front
Reentrant
Backthrusting

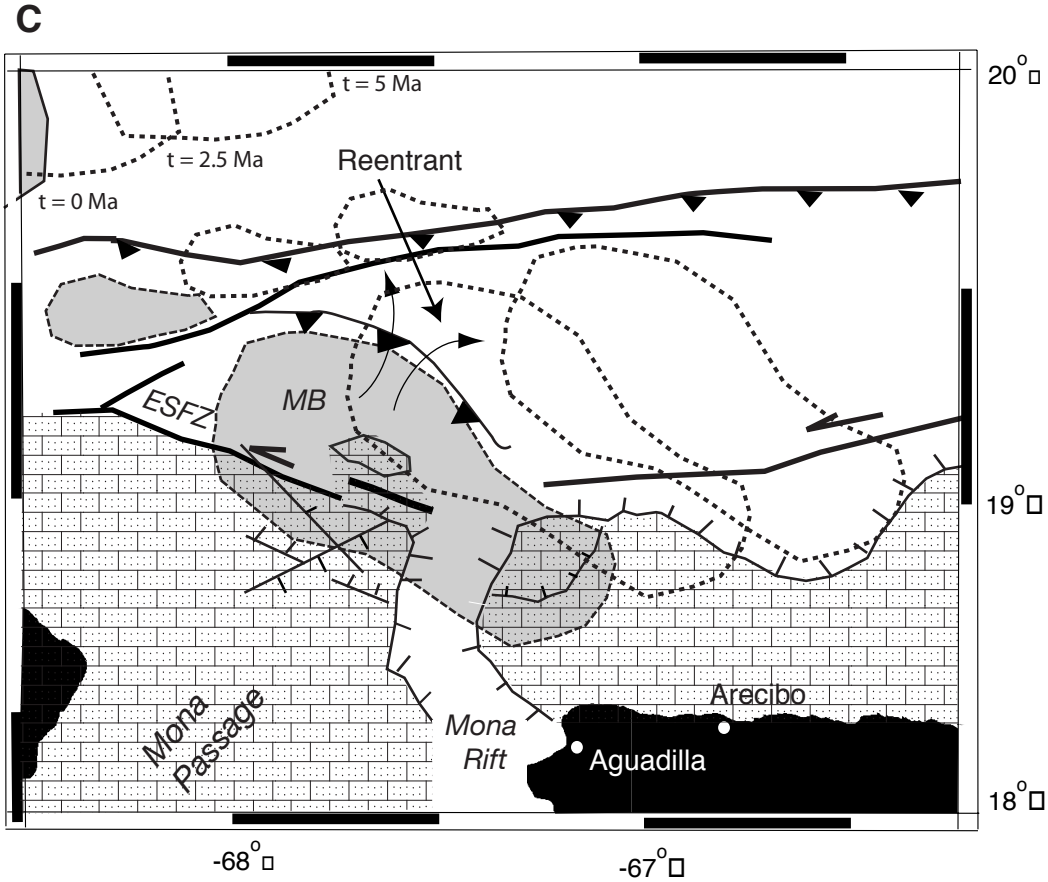
C
t = 5 Ma
t = 2.5 Ma
t = 0 Ma
Reentrant
ESFZ
MB
Mona
Passage
Mona
Rift
Arecibo
Aguadilla
20°
19°
18°
-68°
-67°

APPENDIX A

EW9605 SCS lines 3, 19, 20, and 21 are used to digitize the base-of-landslide horizon and the present seafloor topography using the trace timing application of the Seismic Processing Workshop (SPW). These particular SCS profiles were chosen because they cover the entire area of the headscarp and each line detects the submarine landslide deposits. A fairly continuous, high-amplitude reflector between the arc basement reflections and the overlying seafloor sediments was characterized as the base-of-landslide horizon.

Procedure in SPW:

1. Open the working processing flow for the seismic line of interest.
2. Add card data. Select "horizon file" card data. Link the horizon file to the output file. Double click on the *<filename>.out*.
3. In the SeisViewer window select Trace Timing from the pull-down menu labeled SeisViewer. (Screen capture on the following page).

4. Begin plotting horizon 1 (present seafloor topography) by trace. Our selection began along the amphitheater margin, every 20 traces for the seafloor surface for the extent of the submarine landslide deposit. (Screen capture shown above).
5. Open the horizon card spreadsheet and save.
6. In the seisviewer window, select horizon pick #2 (base-of-landslide deposit). Digitize the extent of the base-of-landslide deposit.
7. Open the horizon card spreadsheet. There should be two fields of data values titled labeled as horizon 1 (present seafloor topography) and horizon 2 (base-of-landslide deposit) (Screen capture on the following page).

8. The horizon file spreadsheet data for each seismic line used is then imported into excel. Excel is used to merge the two-way-travel time data (horizon 1 and horizon 2) with the corresponding geographic coordinates. The EW9605 navigation data (nav file) were supplied from the UTIG online seismic reflection data repository. The final spreadsheet for each seismic line consisted of four columns: horizon 1 two-way-travel time, horizon 2 two-way-travel time, latitude, and longitude. The files were saved as text-only, tab-delimited with line breaks, and merged as one file.

The horizon spreadsheet data were used to make a 2-D grid of the base of the submarine landslide (horizon 2).

APPENDIX B

Digitize Submarine Landslide Extent and Generate Pre-Failure Slope

Step 1:

A 2-D grid of the present seafloor topography (S2) was created using the Generic Mapping Tools (GMT) *grdcut* command line:

grdcut hydro8.clip23.grd -Glandslide.grd -R-67/-66/18:40/19:45 -V

To view this grid in ArcView (vers. 3.2) for purposes of digitization, the new grid was resampled to one of equally x and y dimensions (e.g., 8 arcseconds or 250 meters):

grdsample landslide.grd -Glandslide_resampled.grd -I8c/8c -V

The 2D binary grdfile was converted to an ascii xyz file for input into ArcView:

grd2xyz landslide_resampled.grd -Z > landslide.z

This replaces NaN with –99999 in the bathymetry data:

sed 's/NaN/-99999'/ landslide.z > landslide.asc

Grdinfo was run on the 2D binary grdfile to get grid information (i.e. # cols, # rows...). The xyz ascii file was opened and the following header was inserted as an ascii raster file (.asc):

ncols ##
nrows ##

xllcorner ## (Decimal degrees)

yllcorner ## (Decimal degrees)
cellsize ##
nodata_value –99999

A new view was opened in ArcView and the 3D Image Analysis and Spatial Analyst extensions were turned on. The ascii raster grid was imported and the landslide.grd was added to the view. The project was saved as landslide.apr (project).

Step 2:

The seismic reflection, bathymetry, and sidescan data were used to interpret and digitize the extent of the submarine landslide debris field. In ArcView, the landslide.apr project was opened and the S2 grid (landslide.grd) was made active. Grid contours were added as a shape theme at 100-m intervals. A new point theme was added to the view (avalanche.shp). The theme was made editable and the interpreted extent of the submarine landslide debris field was digitized. The theme attribute table was opened and the new fields: latitude and longitude were inserted. The entire table was selected and the latitude field header was highlighted: calculate > [Shape].GetY. The entire table was selected and the longitude field header was highlighted: calculate > [Shape].GetX. The table was saved. The data were exported as a text file. The text file was used to "mask" the digitized area on the S2 grid in order to generate the isopach map of the landslide debris field (S3).

The extent of the amphitheater-shaped indentation was also digitized. The landslide.apr project was opened and the S2 grid and present-day slope contour theme were activated. A new point theme was added to the view (up_indentation.shp) and the extent of the voided slope area was digitized. The theme attribute table was opened and the new fields, latitude and longitude, were added. The entire table was selected. The latitude field header was highlighted: calculate > [Shape].GetY. The longitude field header was highlighted: calculate > [Shape].GetX. The table was saved and the data were exported as avalanche.txt. The shape file is used for the area and volume calculations of the amphitheater (V1) (Appendix C). The latitude and longitude of the bounding coordinates of the amphitheater area shape file attribute table were exported as a text

file. The text file was imported into the GMT script and used to calculate the area of the seafloor bound by the amphitheater (Appendix C).

Step 3:

To create a 2-D grid of the reconstructed seafloor topography (S1), ArcView and GMT were used. Using GMT, the following grids were combined to get bathymetry with landslide run out as a "hole".

grdmath landslide_resampled.grd avalanche_mask.grd OR = landslide_void.grd

grd2xyz landslide_void.grd -Z > landslide_void.z

sed 's/NaN/-99999'/ landslide_void.z > landslide_mask.asc

landslide_mask.asc was added to the project as a gridded theme.

Final project at this step was the landslide.grd with a void space where avalanche.txt data has been extracted from.

The landslide_mask.grd and contour (at 100-m interval) themes were made active and a new theme was added to the view. The contour data were digitized (Note: each digitized contour needs to have its own attribute table, so for every contour you must add a new theme before you begin digitizing). The contour values over the amphitheater were interpolated across the eastern and western walls of the headscarp, parallel to the slope. The attribute shape file was made active and the new fields: latitude, longitude, and contour were added. The entire table was selected. The latitude field header was highlighted: calculate > [Shape].GetY. The longitude field header was highlighted: calculate > [Shape].GetX. Contour > calculate Type in Contour Numerical Value (i.e. 5600 or 100, etc.). The table was saved. The data were exported as a text file.

All contour attribute tables (x,y, and z data) *<table>.txt* were combined into one text file; pre-failure_contours.txt

The following GMT commands were used to create a 2-D grid of the masked landslide area:

blockmedian pre-fail_contours.txt -R-67/-66/18:40/19:45 -: -I.01 -V > pre-fail_contours.xy

surface pre-fail_contours.xy -Gpre-fail.grd -I.01 -R-67/-66/18:40/19:45 -Tli -T0b -Lu7900 -Ll1900 -: -V

grdfilter pre-fail.grd -Gpre-fail_filter.grd -D0 -Fb0.1 -V

grdsample pre-fail_filter.grd -Gpre-fail2.grd -I8c –V

APPENDIX C

Calculating surface area and volume of indentation and debris deposit.

Step 1: Script used to constrain the surface area of the amphitheater and extent of submarine landslide debris field using Generic Mapping Tools GMT (vers. 3.1).

```
#!/bin/sh
#set -x
# Gridding avalanche base from digitized seismic sections
# There are 4 surfaces to grid (S1 = reconstructed slope; S2 = present-day seafloor topography;
S3 = base-of-landslide deposit; S4 = avalanche surface)

ROOT=/data/prt/meghan/aval                          # Generic name of output
BATH_GRD=/data/prt/meghan/hydro8.clip23.grd     # Bathy grid over avalanche
CONT_AVAL=/data/prt/meghan/aval_revised.txt     # (long, lat) file of avalanche #contour

PAS=0.01              # Grid step in degrees
R=-R-67/-66/18:40/19:45 # Area frame
LAT_MOY=19            # average latitude
VIT=1800       # P-wave average velocity in avalanche for depth conversion

MASK=Y  # Y[es] to mask outside the avalanche
SURF=Y  # Y[es] to calculate the avalanche area
XYZ=Y   # Y[es} tp create a (xyz) file in meters of the avalanche base from digitize seismic
time sections
GRILLE=Y  # Y[es] to grid the avalanche base.
VOL=Y # Y[es] to generate the avalanche isopach grid
VOL2=Y # Y[es] to generate the indentation isopach grid
EP=N   # Y[es} to plot the avalanche isopach grid

gmtset DOTS_PR_INCH 300
gmtset MEASURE_UNIT cm
gmtset COLOR_NAN 255/0/0
gmtset ELLIPSOID Sphere
#NOTE: setting the ellipsoid to sphere will impact psbasemap, grdimage and grdcontour.  #Will
need to reset to WGS-84
#
################################################

case $MASK in
Y )
echo "Create a mask in the digitized polygon surrounding the avalanche"

#To create a grid that when used in grdmath will generate grids showing data only
```

```
#within the avalanche areas (avalance_mask2= entire avalanche;
#up_indentation_mask=indentation; low_indentation_mask=extent of debris flow beyond #base
of slope)
grdmask aval_revised.txt -Gavalanche_mask2.grd -NNaN/NaN/1 -I8c -R-67/-66/18:40/19:45 -:
grdmask up_indentation.txt -Gup_indentation_mask.grd -NNaN/NaN/1 -I8c -R-67/-
66/18:40/19:45 -:
grdmask low_indentation.txt -Glow_indentation_mask.grd -NNaN/NaN/1 -I8c -R-67/-
66/18:40/19:45 -:

;;
esac

################################################
#Calculate surface area of entire avalanche, upper indentation and lower avalanche
case $SURF in
Y )

grdinfo -M -L2 avalanche_mask2.grd > info.grd
# MAKE SURE TO UPDATE THE MEAN LATITUDE OF THE AVLANCHE in the #line that
begins with
COR=cos (lat.*.....

awk ' {
     if (NR == 6) {
       PX=$7 * 111
       NX=$11}
     if (NR == 7) {
       PY=$7 * 111
       NY=$11
       COR=cos(19*3.14159/180)
       S = PX * PY * COR}
     if (NR == 10) {
       NAN=$2
       REAL=(NX*NY)-NAN
       print "Surface area of entire avalance =",  S * REAL, "km2"
       exit }
     }' info.grd


grdinfo -M -L2 up_indentation_mask.grd > info.grd
# MAKE SURE TO UPDATE THE MEAN LATITUDE OF THE AVLANCHE in the #line that
begins with
# COR=cos (lat.*.....

awk ' {
     if (NR == 6) {
```

```
      PX=$7 * 111
      NX=$11}
    if (NR == 7) {
      PY=$7 * 111
      NY=$11
      COR=cos(19*3.14159/180)
      S = PX * PY * COR}
    if (NR == 10) {
      NAN=$2
      REAL=(NX*NY)-NAN
      print "Surface area of upper indentation =",  S * REAL, "km2"
      exit }
    }' info.grd

grdinfo -M -L2 low_indentation_mask.grd > info.grd
# MAKE SURE TO UPDATE THE MEAN LATITUDE OF THE AVLANCHE in the #line that
begins with
# COR=cos (lat.*.....

awk ' {
    if (NR == 6) {
      PX=$7 * 111
      NX=$11}
    if (NR == 7) {
      PY=$7 * 111
      NY=$11
      COR=cos(19*3.14159/180)
      S = PX * PY * COR}
    if (NR == 10) {
      NAN=$2
      REAL=(NX*NY)-NAN
      print "Surface area of lower avalanche =",  S * REAL, "km2"
      exit }
    }' info.grd
;;
esac


################################################
case $XYZ in Y)
echo "Create a file (xyz) with z= avalanche thickness"

echo "L = avalanche thickness is B (surface of avalanche)-E,the depth of the base of the
avalanche "echo  "E*750 m/s + (B-E)*VIT/2 "
```

```
rm -f  BASE_XY

awk  '{print $2, $1, -($3*750+($4-$3)*VIT/2)}' VIT=$VIT/data/prt/meghan/all_horizon2.txt
>BASE_XY


;;
esac

################################################
case $GRILLE in
Y )
  echo "Create grid from digitized depth points. "
  echo "note: take a large grid step and re-sample afterwards. "
  echo "Otherwise it creates artifacts"

rm -f  ${ROOT}_base.grd

blockmedian BASE_XY -I0.1 $R -V > blockmed.xy
surface -T1i -T0b /data/prt/meghan/blockmed.xy -G/data/prt/meghan/surface1.grd -Lu0 -Ll-8850
-I0.01 $R -V
grdfilter /data/prt/meghan/surface1.grd -G/data/prt/meghan/surface1_filt.grd -D0 -Fb.1 -V
grdsample /data/prt/meghan/surface1_filt.grd -G/data/prt/meghan/surface2.grd  -I8c -V
# Now create a grid of the avalanche base only within the avalanche contour
grdmath /data/prt/meghan/surface2.grd avalanche_mask2.grd OR = aval_base.grd
# Now create a grid of the avalanche base within the upper indentation
grdmath /data/prt/meghan/surface2.grd up_indentation_mask.grd OR = upaval_base.grd
# Now create a grid of the avalanche base within lower section
grdmath /data/prt/meghan/surface2.grd low_indentation_mask.grd OR = lowaval_base.grd
# Now create a grid of the avalanche surface bathy within the avalanche contour
grdmath landslide_resampled_neg.grd avalanche_mask2.grd OR = aval_surface.grd
# Now create a grid of the avalanche surface bathy within the upper indentation
grdmath landslide_resampled_neg.grd up_indentation_mask.grd OR = upaval_surface.grd
# Now create a grid of the avalanche surface bathy within the lower section
grdmath landslide_resampled_neg.grd low_indentation_mask.grd OR = lowaval_surface.grd
#grdmath reconstructed_slope.grd -1.0 MUL = reconstructed_slope_neg.grd
#Now create a grid of the reconstructed surface bathy within the avalanche contour
grdmath reconstructed_slope_neg.grd avalanche_mask2.grd OR = aval_reconstructed.grd
grdmath reconstructed_slope_neg.grd up_indentation_mask.grd OR = upaval_reconstructed.grd
grdmath reconstructed_slope_neg.grd low_indentation_mask.grd OR =
lowaval_reconstructed.grd

#rm -f  surface1.grd

;;
esac
```

```
################################################
case $VOL in
Y )
echo  "Generate ${ROOT}_diff.grd"
echo "Substract avalanche base from avalanche surface and convert to km"
grdmath aval_surface.grd aval_base.grd SUB 1000 DIV = aval_diff.grd
grdmath upaval_surface.grd upaval_base.grd SUB 1000 DIV = upaval_diff.grd
grdmath lowaval_surface.grd lowaval_base.grd SUB 1000 DIV = lowaval_diff.grd
;;
esac
############################################################
case $VOL2 in
Y)
# Generate isopach grid of the voided area by subtracting the present topography from the
#reconstructed
pre-indentation topography

echo  "Generate grid of voided area"
echo "Substract present topo from reconstructed and convert to km"
# First for the entire avalanche
grdmath aval_reconstructed.grd aval_surface.grd SUB 1000 DIV = aval_void.grd
# Now, just for the upper indentation
grdmath upaval_reconstructed.grd upaval_surface.grd SUB 1000 DIV = upaval_void.grd


################################################
case $EP in
Y )
PSF=aval_thick.ps
J=-Jm15
#gmtset ELLIPSOID WGS-84
#Plot the avalanche thickness as an isopach map

echo "avalanche thickness"
grdmath aval_surface.grd aval_base.grd SUB  = ${ROOT}_thick.grd

grdcontour ${ROOT}_thick.grd $J $R -C250 -A500 -Wc.5 -Wa1 -V -K -P -Y4 -X2 >$PSF
psxy up_indentation.txt $J $R -O -K -W.5/0/255/0 -V -:  >> $PSF
psxy low_indentation.txt $J $R -O -K -W.5/255/0/0 -V -:  >> $PSF
#psxy aval_revised.txt $J $R -O -K -W.5/255/255/0 -V -:  >> $PSF
psbasemap $J -R -Ba.5f:."Thickness of the Avalanche Deposit in meters": -O >> $PSF

xpsview $PSF &

;;
```

esac

##

Step 2: Calculate volume of indentation and debris deposit. GMT (3.1) command used to calculate indentation and submarine landslide debris volume. Cut the indentation and debris field into 300-m thick slices to take into account variation in bathymetry. Sum of slice volumes gives volume for entire indentation and debris field

grdvolume aval_diff.grd –Sk –Vl –C 0/2.85014/.3 >result.d

grdvolume upaval_void.grd –Sk –Vl –C0/2.85014/.3 >result2.d

Note: *grdvolume* the area inside the contour line, which is above the contour. Use grid volume to calculate the volume (and area) between each contour and then subtract the result.

Output is four columns:
1st value = specified contour
2nd value = area inside the contour
3rd value = volume inside the contour and under the surface
4th value = maximum mean height (3rd value/2nd value)